TET2–BCLAF1 transcription repression complex epigenetically regulates the expression of colorectal cancer gene Ascl2 *via* methylation of its promoter

Received for publication, October 29, 2021, and in revised form, May 17, 2022 Published, Papers in Press, June 3, 2022,
https://doi.org/10.1016/j.jbc.2022.102095

Yangyang Shang[1], Tao Jiang[1], Lijian Ran[1], Wenjing Hu[1], Yun Wu[1], Jun Ye[2], Zhihong Peng[1], Lei Chen[1], and Rongquan Wang[1,*]

From the [1]Institute of Gastroenterology of PLA, Southwest Hospital, Army Medical University (Third Military Medical University), Chongqing, China; [2]Department of Gastroenterology of 958 Hospital, Army Medical University (Third Military Medical University), Chongqing, China

Edited by Eric Fearon

Ascl2 has been shown to be involved in tumorigenesis in colorectal cancer (CRC), although its epigenetic regulatory mechanism is largely unknown. Here, we found that methylation of the *Ascl2* promoter (bp -1670 ∼ -1139) was significantly increased compared to the other regions of the *Ascl2* locus in CRC cells and was associated with elevated *Ascl2* mRNA expression. Furthermore, we found that promoter methylation was predictive of CRC patient survival after analyzing DNA methylation data, RNA-Seq data, and clinical data of 410 CRC patient samples from the MethHC database, the MEXPRESS database, and the Cbioportal website. Using the established TET methylcytosine dioxygenase 2 (TET2) knockdown and ectopic TET2 catalytic domain–expression cell models, we performed glucosylated hydroxymethyl–sensitive quatitative PCR (qPCR), real-time PCR, and Western blot assays to further confirm that hypermethylation of the *Ascl2* promoter, and elevated *Ascl2* expression in CRC cells was partly due to the decreased expression of TET2. Furthermore, BCLAF1 was identified as a TET2 interactor in CRC cells by LC-MS/MS, coimmunoprecipitation, immunofluorescence colocalization, and proximity ligation assays. Subsequently, we found the TET2–BCLAF1 complex bound to multiple elements around CCGG sites at the *Ascl2* promoter and further restrained its hypermethylation by inducing its hydroxymethylation using chromatin immunoprecipitation-qPCR and glucosylated hydroxymethyl-qPCR assays. Finally, we demonstrate that TET2-modulated *Ascl2*-targeted stem gene expression in CRC cells was independent of Wnt signaling. Taken together, our data suggest an additional option for inhibiting *Ascl2* expression in CRC cells through TET2–BCLAF1–mediated promoter methylation, Ascl2-dependent self-renewal of CRC progenitor cells, and TET2–BCLAF1–related CRC progression.

Studies have investigated the genes and encoded proteins involved in the maintenance of stemness in colorectal cancer (CRC) cells, which contain a population of CRC progenitor cells (1–3). Indeed, it is important to identify the regulatory mechanisms involved in CRC cells to develop novel reagents that target stemness (4).

Achaete scute-like 2 (Ascl2), a basic helix-loop-helix transcription factor (TF), is a downstream target of Wnt signaling. Ascl2 may be a regulatory factor that controls the fate of intestinal Lgr5$^+$ crypt-based stem cells and CRC progenitor cells (5–7). It has also been found to initiate T helper cell development, differentiation from mouse trophoblast stem cells to trophoblast progenitors, and intestinal neoplastic epithelial cell differentiation to a goblet cell phenotype (8–10). However, the molecular mechanism of Ascl2 overexpression in CRC progenitor cells is still unclear. Wnt signaling enhances Ascl2 autoregulation and cobinding to the Ascl2 promoter by the YAP1–Krüppel-like Factor 5 (KLF5) complex, and hypoxia inducible factor-1α (HIF-1α) forms a transcriptional switch to activate Ascl2 expression (11–13). This mechanism has an impact on the self-renewability of CRC progenitor cells.

Aberrant DNA methylation is related to altered gene expression patterns and is a fundamental feature of cancer (14). It is commonly known that a cancer-specific redistribution of DNA methylation occurs, including global hypomethylation punctuated by regional hypermethylation of gene promoters (14, 15), and this regional hypermethylation of gene promoters leads to the upregulation of paradoxical gene activation in cancer (16, 17). This finding seems to be contradictory to the classical knowledge in which dense promoter DNA methylation is associated with transcriptional repression (18). There is increasing recognition that this paradigm drives the evolution of malignancy. Reversing DNA methylation abnormalities by targeting the maintenance DNA methylation machinery represents a potential therapeutic strategy for treating malignancy (19, 20).

Epigenetic modification has fundamental roles in defining unique cellular identity through the establishment and maintenance of lineage-specific chromatin and methylation status (21, 22). DNA modifications, such as 5-hydroxymethylcytosine (5hmC), are catalyzed by ten-eleven-translocation (TET) enzyme (TET1-3) methylcytosine dioxygenase family members, and the roles of TET proteins in regulating chromatin

* For correspondence: Rongquan Wang, rongquanw@hotmail.com.

architecture and gene transcription independent of DNA methylation have been gradually uncovered (23, 24). TET2 is frequently mutated in hematological malignancies (25, 26), and patients carrying TET2 mutations often show significantly reduced global 5hmC levels (27). Interestingly, loss of 5hmC is also observed in many solid tumors (28–30), where TET2 mutations are rarely detected (19). However, how TET2 inactivation and loss of 5hmC affect promoter or enhancer methylation has been controversial (27, 31–35).

Little is known about the epigenetic regulatory mechanism regulating Ascl2 expression in CRC. In this study, we found an interesting epigenetic regulatory mechanism of Ascl2 in CRC. Using the MethHC database (http://methhc.mbc.nctu.edu.tw) and other sources to mine gene methylation data, we identified that there was a region (transcription start site [TSS] 1500: −1670 ∼ −1139) in Ascl2 promoter with higher methylation level comparing with the other regions of the Ascl2 locus in CRC samples and was associated with Ascl2 mRNA expression and predicted CRC patient survival. We now proposed a new mechanism of TET2–Bcl-2-associated transcription factor 1 (BCLAF1)–mediated Ascl2 TSS1500 promoter demethylation, which was involved in modulating Ascl2 overexpression in CRC cells. The epigenetic modification of Ascl2 promoter in CRC cells may represent another mechanism to control Ascl2-dependent CRC cell fate. Our present data thus also suggested an additional option for inhibiting Ascl2 expression in CRC, Ascl2-dependent self-renewal of CRC progenitor cells and TET2–BCLAF1 complex–related CRC progression.

Results

DNA methylation pattern of the Ascl2 locus and its correlation with Ascl2 mRNA levels in CRC tissues

We downloaded DNA methylation data from the MethHC database and then compared the methylation levels across the Ascl2 locus between cancerous samples (n = 369) and normal colon mucosa tissues (n = 45) from CRC patients. The Ascl2 locus included an upstream Ascl2 promoter located -1500 nt before the TSS, which was defined as TSS1500; an upstream Ascl2 promoter located 200 nt before the TSS, which was defined as TSS200; a 5′-UTR; the first exon; and a 3′-UTR. The methylation level in the Ascl2 TSS1500 promoter was significantly higher than that of TSS200, the 5′-UTR, the first exon, and the 3′-UTR in CRC samples, and there was higher methylation level in this region (-1670 ∼ -1139) of Ascl2 promoter comparing cancerous tissues with normal colon mucosa tissues (Fig. 1*A*). We screened for methylated CpGs across the Ascl2 locus and found that they were significantly associated with Ascl2 mRNA expression in 410 CRC samples from the MEXPRESS database. Interestingly, the methylation levels of some CpGs located in TSS1500 were positively correlated with Ascl2 mRNA expression, while the methylation levels of CpGs in other regions were inversely correlated with Ascl2 mRNA expression (Fig. S1).

The UCSC Genome Browser (http://genome.ucsc.edu/cgi-bin/hgGateway) tracks showed the Ascl2 locus and a hypermethylation status in the Ascl2 TSS1500 promoter from Infinium/Illumina 450K methylation array data analysis of Caco-2 colon cancer cells (*orange color*, beta value ≥ 0.6) (Fig. 1*B*). Methylated CpGs significantly associated with Ascl2 expression are marked by array probes (Fig. 1*B*), and the methylation levels between cancerous and normal colon mucosa tissues are compared from the MEXPRESS database (Fig. 1*C*). Among the 26 methylated CpGs related to Ascl2 expression, 23 differentially methylated CpGs (DMCs) had different methylation levels between cancerous and normal colon mucosa tissues (Fig. 1*C*). DMCs in TSS1500 of the Ascl2 locus marked as *red text* showed a hypermethylation status in the CRC samples (Fig. 1*C*).

Ascl2 TSS1500 promoter DMC methylation levels predicted CRC patient survival

In addition to our global analysis of DMCs in TSS1500 of the Ascl2 locus of human CRC, we also used TCGA gene expression and clinical data to determine how well Ascl2 TSS1500 promoter DMC methylation levels predict CRC patient outcome by dividing the beta values of each DMC into low- and high-methylation groups using Kaplan–Meier survival analysis (Fig. S2). The log-rank test results showed that three out of eight DMCs at Ascl2 TSS1500 marked as *purple dots* were significantly associated with both overall survival (OS) and disease-free survival (DFS) of patients ($p < 0.05$, hazard ratio > 1). These three DMCs were cg01156550, cg20392764, and cg21063716. Their methylation level, T stage, N stage, and AJCC stage in CRC patients were all prognostic factors for OS and DFS of CRC patients ($p < 0.05$, hazard ratio > 1), among which cg20392764 was an independent prognostic factor (OS: $p = 0.006$, hazard ratio = 2.773; DFS: $p = 0.037$, hazard ratio = 1.789), suggesting that the methylation status of cg01156550, cg20392764, and cg21063716 residing at the Ascl2 TSS1500 promoter played a crucial role in CRC prognosis (Fig. S2).

Ascl2 TSS1500 promoter hydroxymethylation was related to its methylation level and Ascl2 expression in human CRC tissues

Cytosine methylation of CpGs is the major epigenetic modification of mammalian DNA and plays important roles in development and cancer. Loss of TET family associated 5hmC is concomitant with aberrant promoter hypermethylation in cancer cells (36). In CRC, a global reduction in 5hmC is an obvious phenomenon (37).

To determine the roles of 5hmC and 5-methylcytosine (5mC) in aberrant expression of Ascl2 in CRC tissues, we analyzed the potential 5hmC/5mC sites containing CCGG (P1-P4) in the genome from cg01156550 to cg12499235 residing in the TSS1500 promoter region (Fig. 2*A*) and detected site-specific levels of 5hmC and 5mC in human CRC samples and their paired pericancerous tissues (n = 7) by using glucosylated hydroxymethyl (GluMS)–sensitive quatitative PCR (qPCR), as well as Ascl2 mRNA levels in human CRC samples and their pericancerous tissues by using real-time

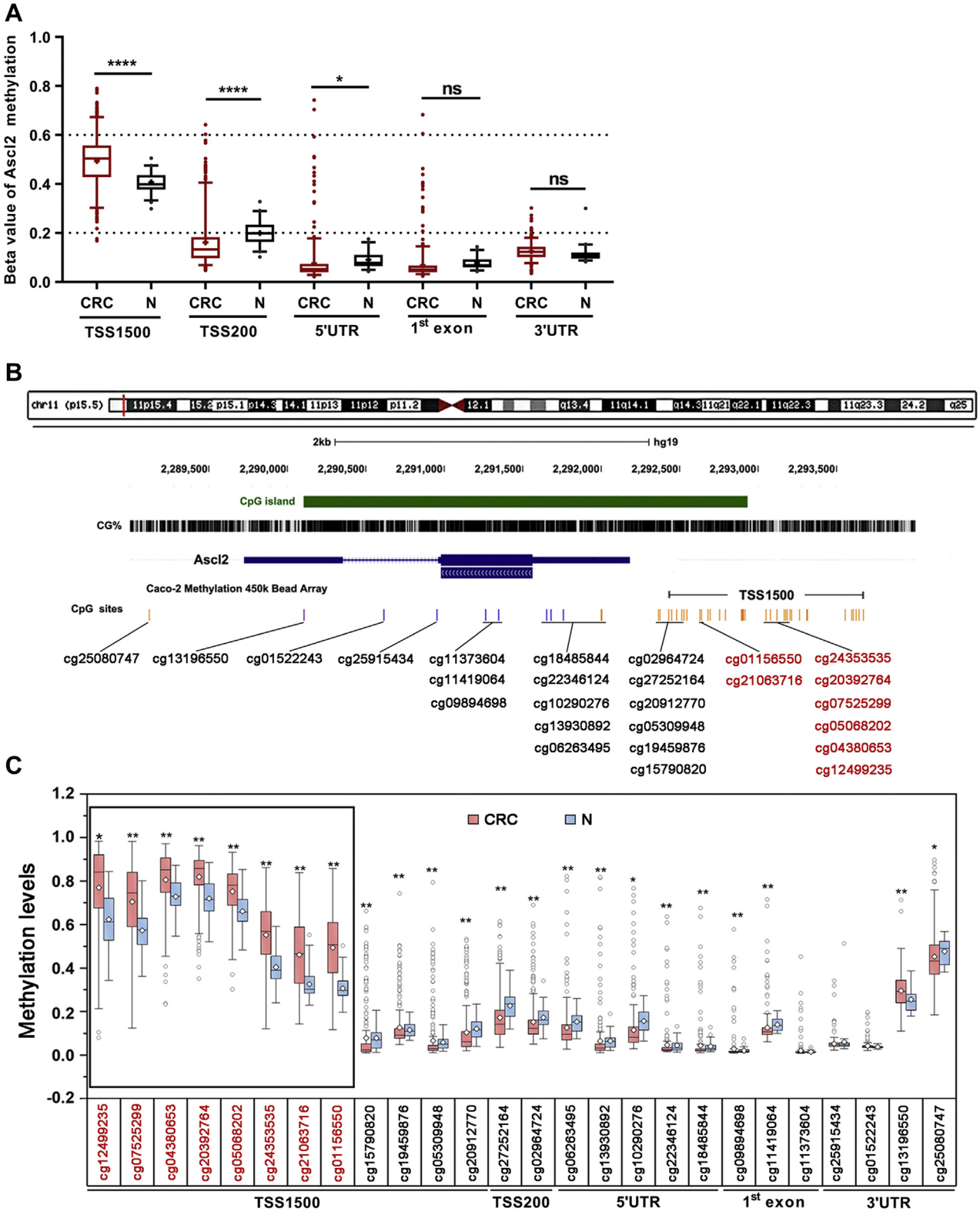

Figure 1. The DNA methylation pattern of the Ascl2 locus in colorectal cancer from the TCGA database. *A*, methylation levels differed across the different regions of the Ascl2 locus (TSS1500, TSS200, 5′-UTR, first exon, and 3′-UTR) between cancerous and normal colon mucosa tissues from CRC patients. The *y*-axis indicates beta value: scores in the range between 0 and 1 indicate the level of DNA methylation. *B*, UCSC screenshot of the Ascl2 locus and distribution of differentially methylated CpGs (DMCs) from TSS1500 to the 3′-UTR within Ascl2 locus are shown in their approximate location. *C*, comparison of the methylation levels of DMCs distributed from TSS1500 to the 3′-UTR across the Ascl2 locus between CRC and normal colon tissues. The *red text* indicates DMCs in TSS1500 of the Ascl2 locus. $^{ns}p > 0.05$, $^{*}p < 0.05$, $^{**}p < 0.01$, $^{***}p < 0.001$, $^{****}p < 0.0001$, unpaired two-tailed Student's *t* test. CRC, colorectal carcinoma; TSS: transcriptional start site.

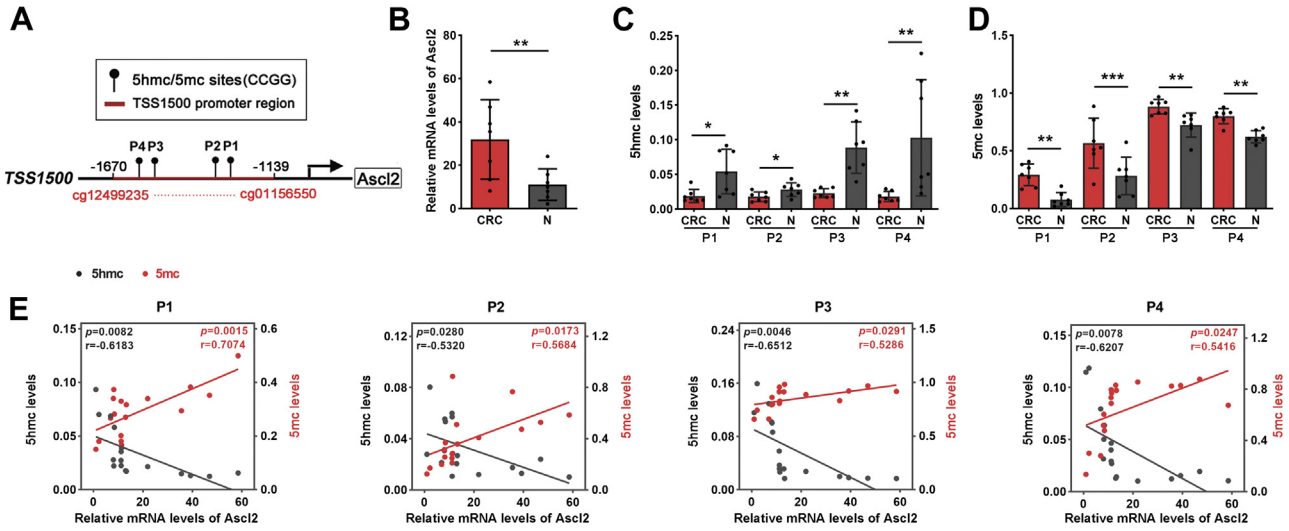

Figure 2. Hydroxymethylation of the Ascl2 TSS1500 promoter was related to its methylation level and Ascl2 expression. *A*, schematic diagram of the Ascl2 TSS1500 promoter. The *black circles* above the *solid line* (P1, P2, P3, and P4) represent the potential 5hmC/5mC sites containing CCGG in the genome from cg01156550 to cg12499235 residing in the TSS1500 promoter region. *B*, Ascl2 mRNA levels in the human CRC samples (n = 7) quantitated by real-time PCR were significantly higher than those of the paired pericancerous mucosa derived from endoscopic biopsy. $^{**}p < 0.01$, paired two-tailed student's *t* test. *C* and *D*, site-specific levels of 5hmC and 5mC at TSS1500 of the Ascl2 promoter in human CRC samples (n = 7) and their paired pericancerous tissues were determined by using GluMS-qPCR. *E*, correlation analysis was performed for Ascl2 mRNA levels and methylation levels at P1 to P4, as well as Ascl2 mRNA levels and hydroxymethylation levels at P1 to P4. $^{*}p < 0.05$, $^{**}p < 0.01$, $^{***}p < 0.001$, unpaired two-tailed Student's *t* test. 5hmC, 5-hydroxymethylcytosine; CRC, colorectal cancer; GluMS, glucosylated hydroxymethyl–sensitive; qPCR, quatitative PCR; TSS, transcription start site.

PCR. The Ascl2 mRNA level in CRC tissues was significantly higher than that in pericancerous tissues ($p < 0.01$) (Fig. 2*B*). The P1, P2, P3, and P4 site-specific levels of 5hmC at Ascl2 TSS1500 promoter in human CRC samples were lower than those in pericancerous tissues ($p < 0.05$ or $p < 0.01$) (Fig. 2*C*), and the P1, P2, P3, and P4 site-specific levels of 5mC at Ascl2 TSS1500 promoter in human CRC samples were higher than those in pericancerous tissues ($p < 0.01$ or $p < 0.001$) (Fig. 2*D*). Correlation analysis for Ascl2 mRNA levels and methylation levels at P1 to P4 indicated a positive correlation, whereas there was an inverse correlation between Ascl2 mRNA levels and hydroxymethylation levels at P1 to P4 (n = 17) (Fig. 2*E*). These primary results indicated that DNA hypermethylation at a specific site of the Ascl2 TSS1500 promoter could be related to the reduced hydroxymethylation at these sites and be responsible for altered Ascl2 expression. Furthermore, we focused on confirmation of its mechanism.

TET2 was inversely correlated with Ascl2 expression in CRC samples and CRC cell lines

Altered hydroxymethylation levels were attributed to inactivation or abnormal expression of TET proteins. We compared TET1, TET2, TET3, and Ascl2 mRNA levels in human CRC samples and their pericancerous mucosa from the TCGA RNA-Seq database and found that TET2 mRNA level in human CRC samples was significantly lower than their pericancerous mucosa, and Ascl2 mRNA level in human CRC samples was significantly higher than their pericancerous mucosa ($p < 0.0001$, Fig. 3*A*), whereas there was no significant difference in TET1 and TET3 mRNA levels between human CRC samples and their pericancerous mucosa (data not shown). Correlation analysis of TET2 and Ascl2 mRNA levels in human CRC samples from the TCGA RNA-Seq database indicated that TET2 mRNA levels in CRC tissues were inversely correlated with Ascl2 mRNA levels (R = −0.5064, $p < 0.0001$, Fig. 3*B*). TET2 and Ascl2 mRNA levels in HCT116, LOVO, SW480, and SW620 colon cancer cells were quantified by real-time PCR and were inversely correlated (R = −0.8946, $p < 0.0001$, Fig. 3, *C* and *D*). TET2 and Ascl2 protein levels in four kinds of colon cancer cells detected by Western blot and assessed by ImageJ software (https://imagej.nih.gov/ij/) indicated that those cells with high TET2 protein expression had low Ascl2 protein expression (Fig. 3, *E* and *F*). Ascl2 mRNA and protein levels in colon cancer cells after exposure to hydroxymethylase inducer vitamin C for 0 to 4 h were decreased but partially recovered at 8 h after exposure to vitamin C. Ascl2 mRNA and protein levels in colon cancer cells after exposure to hydroxymethylase inhibitor dimethyloxalylglycine (DMOG) or deferoxamin (DFO) for 0 to 8 h were increased (Fig. 3,*G–I*). The current data indicated the possible role of TET2-mediated hydroxymethylation in regulating Ascl2 expression.

TET2 suppressed Ascl2 expression by regulating 5hmC and 5mC levels of the Ascl2 TSS1500 promoter

To confirm whether TET2 regulates Ascl2 expression, we first established two stable TET2-knockdown HCT116 cells and SW480 cells and two stable SW620 cell line ectopically expressing WT TET2 catalytic domain or mutated TET2 catalytic domain with mutation of the HxD motif, which is located in the core double-stranded β-helix domain in the TET2 catalytic domain (H1382/Y and D1384A) (Fig. 4*A*). Next, we examined TET2 and Ascl2 mRNA and protein levels in the TET2-knockdown HCT116 cells and SW480 cells by

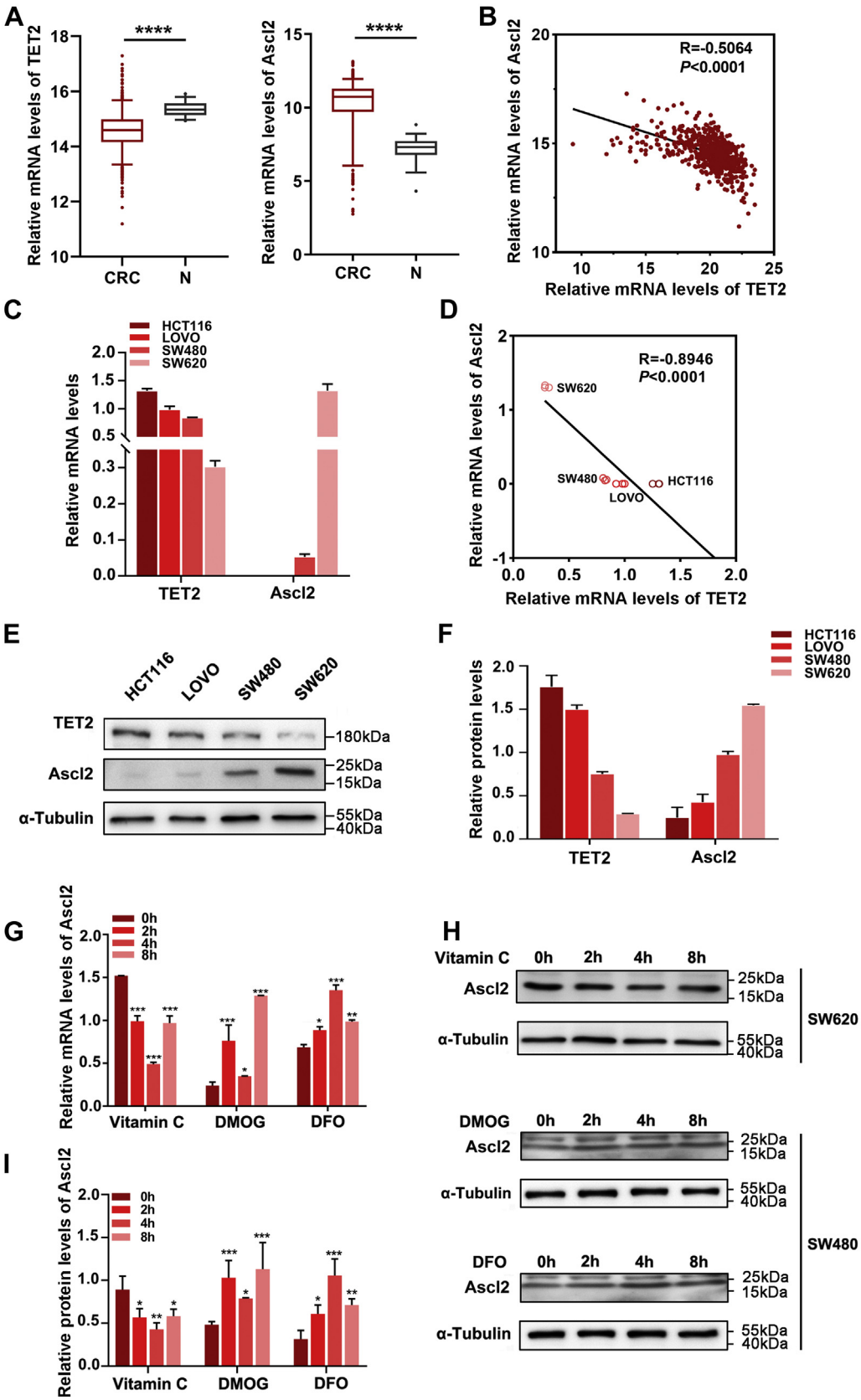

Figure 3. TET2 expression in CRC tissues was downregulated and inversely correlated with Ascl2 mRNA levels. *A*, TET2 and Ascl2 mRNA levels in human CRC samples and their paired pericancerous mucosa from the TCGA RNA-Seq database. *B*, correlation analysis between TET2 and Ascl2 mRNA levels in CRC tissues. *C*, TET2 and Ascl2 mRNA levels in four kinds of colon cancer cells were determined by quantitative real-time PCR (n = 3). *D*, correlation analysis between the mRNA expression of TET2 and Ascl2 in four kinds of colon cancer cells (n = 3). *E* and *F*, TET2 and Ascl2 protein levels in four kinds of colon cancer cells were determined by Western blot and assessed by Image J software (n = 3). *G–I*, Ascl2 mRNA and protein levels in colon cancer cells were determined by quantitative real-time PCR (*G*) and Western blot (*H*) in different periods after exposure to the hydroxymethylase inhibitors DMOG and DFO

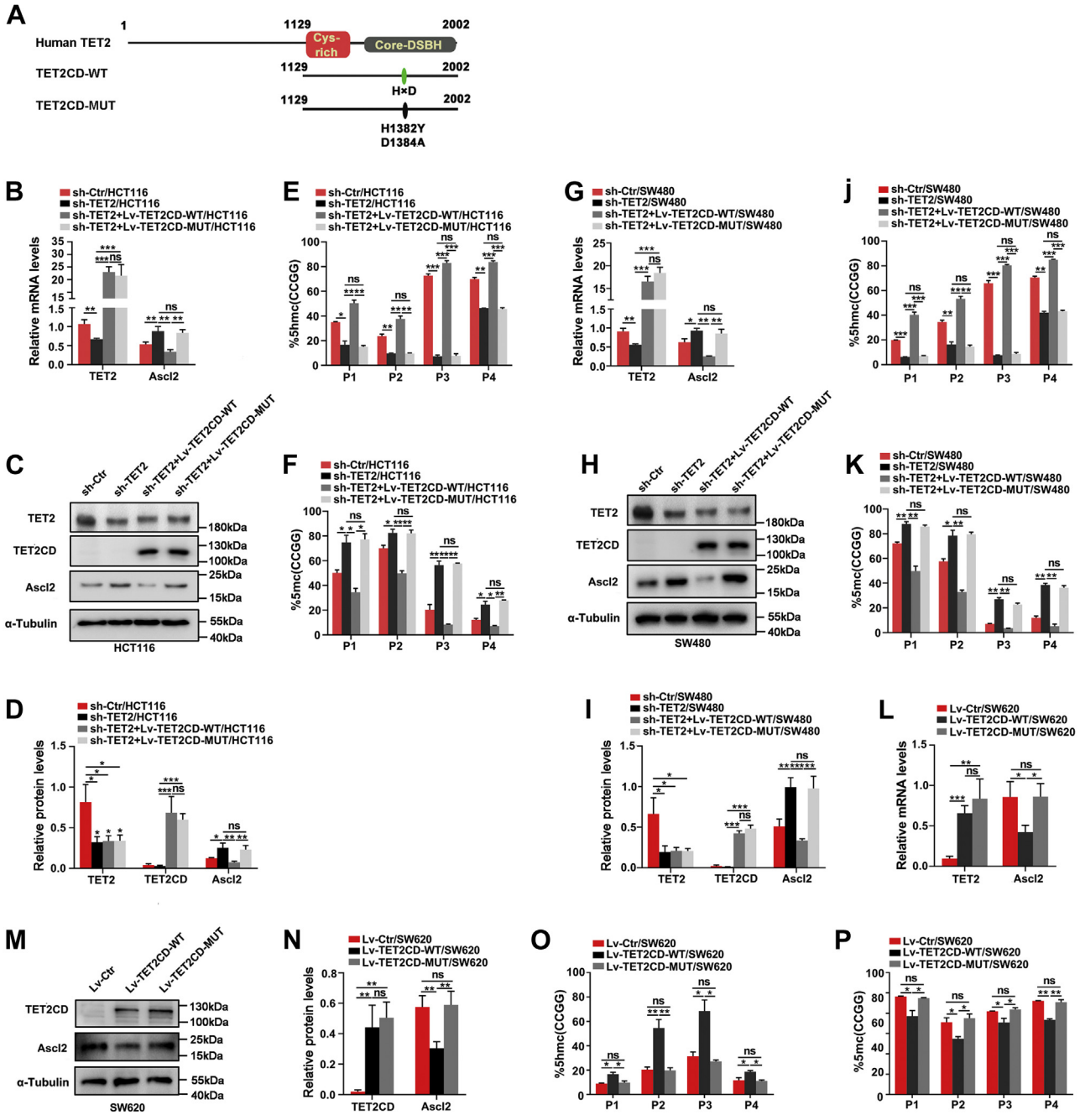

Figure 4. TET2 suppressed Ascl2 expression by regulating 5hmC and 5mC levels of the Ascl2 TSS1500 promoter. *A*, schematic diagram of TET2 construct. The core DSBH domain harbors an HxD motif that interacts with Fe (II) and 2OG and is a key catalytic motif for TET2. The mutated TET2 catalytic domain (TET2CD-MUT) carried two critical mutations (H1382/Y and D1384A) in the HxD motif compared with the WT TET2 catalytic domain (TET2CD-WT). *B–K*, TET2 and Ascl2 mRNA and protein levels in stable TET2-knockdown HCT116 cells and stable TET2-knockdown HCT116 cells overexpressing TET2CD-WT or TET2CD-MUT (*B–D*) and stable TET2-knockdown SW480 cells and stable TET2-knockdown SW480 cells overexpressing TET2CD-WT or TET2CD-MUT (*G–I*) were determined by quantitative real-time PCR and Western blot, respectively, and the site-specific levels of 5hmC and 5mC at TSS1500 of the Ascl2 promoter in aforementioned cells were determined by using GluMS-qPCR (*E*, *F*, *J*, and *K*). *L–N*, TET2 and Ascl2 mRNA and protein levels in stable SW620 cells overexpressing TET2CD-WT or TET2CD-MUT were determined by quantitative real-time PCR and Western blot, respectively, and the site-specific levels of 5hmC and 5mC at TSS1500 of the Ascl2 promoter in aforementioned cells were determined by using GluMS-qPCR (*O* and *P*). The protein levels in Western blot were assessed by ImageJ (n = 3) (*D*, *I*, and *N*). *$p < 0.05$, **$p < 0.01$, ***$p < 0.001$, $^{ns}p > 0.05$, unpaired two-tailed Student's *t* test. 5hmC, 5-hydroxymethylcytosine; GluMS, glucosylated hydroxymethyl–sensitive; qPCR, quatitative PCR; TSS, transcription start site.

real-time PCR and Western blot assays. We found that reduced TET2 expression resulted in increased Ascl2 expression, and enforced expression of the TET2 catalytic domain in the TET2-knockdown HCT116 cells and SW480 cells led to a reduction in Ascl2 expression, while mutated TET2 catalytic domain with mutation of the HxD motif failed to reduce Ascl2

and the hydroxymethylase inducer vitamin C, respectively. Their Ascl2 protein levels in Western blot were assessed by ImageJ (n = 3) (*I*). *$p < 0.05$, **$p < 0.01$, ***$p < 0.001$, ****$p < 0.0001$, unpaired two-tailed Student's *t* test. CRC, colorectal cancer; DFO, deferoxamin; DFS, disease-free survival.

expression (Fig. 4, *B–D*, *G* and *I*), suggesting that TET2-mediated Ascl2 expression was dependent on the TET2 catalytic domain.

Moreover, we performed GluMS-qPCR to quantify the specific-site 5hmC and 5mC levels at the P1 to P4 locus on Ascl2 TSS1500 promoter and found that TET2 knockdown led to a significant decrease in 5hmC levels and an increase in 5mC levels at the P1 to P4 locus. Ectopic expression of the TET2 catalytic domain in the TET2-knockdown HCT116 cells and SW480 cells significantly increased 5hmC levels and reduced 5mC levels at the P1 to P4 locus, while the mutant TET2 catalytic domain, which disturbed their catalytic activity in oxidizing 5mC, failed to increase 5hmC levels and recovered their 5mC levels at the P1 to P4 locus (Fig. 4, *E*, *F*, *J* and *K*).

Enforced expression of the TET2 catalytic domain in SW620 cells led to a reduction in Ascl2 expression, while mutated TET2 catalytic domain failed to reduce Ascl2 expression (Fig. 4, *L* and *N*). Ectopic expression of the TET2 catalytic domain in SW620 cells significantly increased 5hmC levels and reduced 5mC levels at the P1 to P4 locus, while the mutant TET2 catalytic domain failed to increase 5hmC levels and recovered their 5mC levels at the P1 to P4 locus (Fig. 4, *O* and *P*).

These results confirmed that TET2 suppressed Ascl2 expression by regulating 5hmC and 5mC levels residing in the Ascl2 TSS1500 promoter.

TET2 modulated the CRC stemness phenotypes independent of Wnt signaling

We examined the mRNA levels of several stemness genes in stable TET2-knockdown SW480 and HCT116 cells and stable SW620 cells with ectopic TET2 catalytic domain expression or mutated TET2 catalytic domain expression. The data showed that TET2 knockdown resulted in an increase of multiple stemness genes expression, and forced TET2 catalytic domain expression inhibited their expression of these genes, while the mutant TET2 catalytic domain weakened the TET2 catalytic domain effect on their expression (Fig. 5*A*). Flow cytometry assays revealed that stable TET2-knockdown SW480 and HCT116 cells had an increased proportion of $CD44^+$ cells and $CD133^+$ cells (72.08% and 73.31%) compared with their control cells (25.72% and 31.02%), respectively. Stable SW620 cells with the WT TET2 catalytic domain had a decreased proportion of $CD133^+$ cells (25.90%) compared with their control cells (90.79%), while stable SW620 cells with the mutant TET2 catalytic domain had a similar proportion of $CD133^+$ cells as their control cells (89.99% *versus* 90.79%) (Fig. 5*B*). Stable TET2-knockdown SW480 and HCT116 cells exhibited an increased tumorsphere potential compared with their control cells. Stable SW620 cells with ectopic expression of WT TET2 catalytic domain had a decreased tumorsphere potential compared with their control cells, while stable SW620 cells with the mutant TET2 catalytic domain exhibited tumorsphere potential similar to that of their control cells (Fig. 5, *C* and *D*). Vitamin C enhanced the inhibitory effect of the TET2 catalytic domain on tumorsphere formation compared with its control cells (Fig. S3). *In vivo* tumorigenicity showed that stable SW620 cells with the WT TET2 catalytic domain had reduced tumor volume and weight compared with their control cells, while its mutant had no significant effect on tumor volume and weight (Fig. 5, *E–G*). The aforementioned results indicated that TET2 could repress the expression of stemness genes and the stemness phenotypes of CRC cells.

Ascl2 is the target of Wnt signaling (38), whereas, the zinc finger TF PLAGL2 activates Ascl2 expression independent of canonical Wnt signaling (39), whether TET2 regulates Ascl2 expression through Wnt signaling remains unclear. We first analyzed the RNA-Seq data for CRC tumors from the TCGA database according to Wnt-activating mutations (truncating mutations in APC or AXIN2 or missense mutations in β-catenin) (40). The correlation coefficient of Ascl2 and TET2 expression presented no obvious change between Wnt mutant ($R = -0.4755$, $p < 0.0001$) and nonmutant CRC tumors ($R = -0.4325$, $p < 0.0001$) (Fig. 5, *H* and *I*). Next, we examined the mRNA levels of Ascl2 and the other stemness genes in stable TET2-knockdown SW480 and HCT116 cells treated with IWP-2, an inhibitor that selectively blocks porcine-mediated Wnt palmitoylation and does not affect Wnt/β-catenin, which significantly inhibited the transcriptional levels (mRNA) of two canonical Wnt target genes Axin2 and Twist (Fig. 5*J*). After 72 h of 2 μM IWP-2 treatment, the mRNA levels of Ascl2 and its downstream Cdca7, c-*myc*, Lgr5, and Sox9 were still increased in stable TET2-knockdown SW480 and HCT116 cells (Fig. 5*K*), suggesting that TET2 regulated Ascl2 and Ascl2 downstream stemness genes independently of canonical Wnt signaling.

TET2-Ascl2 axis modulated CRC stemness phenotypes

Because of the TET2 effect on Ascl2 expression and the critical role of Ascl2 in CRC stem cells, we hypothesized that TET2 might regulate the phenotypes of CRC stem cells by modulating the expression of CRC cell stemness genes. We examined the mRNA and protein levels of Ascl2 and its downstream stemness genes using real-time PCR and Western blot in stable SW620 cells overexpressing the WT TET2CD and stable SW620 cells overexpressing the WT TET2CD and heterologous Ascl2. Forced TET2 catalytic domain expression inhibited the expression of Ascl2 and its downstream stemness-related genes, including Cdca7, c-*myc*, Lgr5, and Sox9, ectopic expression of Ascl2 for 72 h in stable SW620 cells with the TET2 catalytic domain significantly restored the expression of Ascl2 and its downstream stemness genes at both the mRNA and protein levels (Fig. 6, *A* and *B*). Flow cytometry assays for $CD133^+$ cells revealed that stable SW620 cells overexpressing the TET2 catalytic domain had a decreased proportion of $CD133^+$ cells (40.05%) compared with their control cells (79.04%), but there were almost 91.06% $CD133^+$ cells in stable SW620 cells with TET2 catalytic domain and heterologous Ascl2 expression (C). Stable SW620 cells with the TET2 catalytic domain had an inhibited tumorsphere formation, while its forced Ascl2 expression

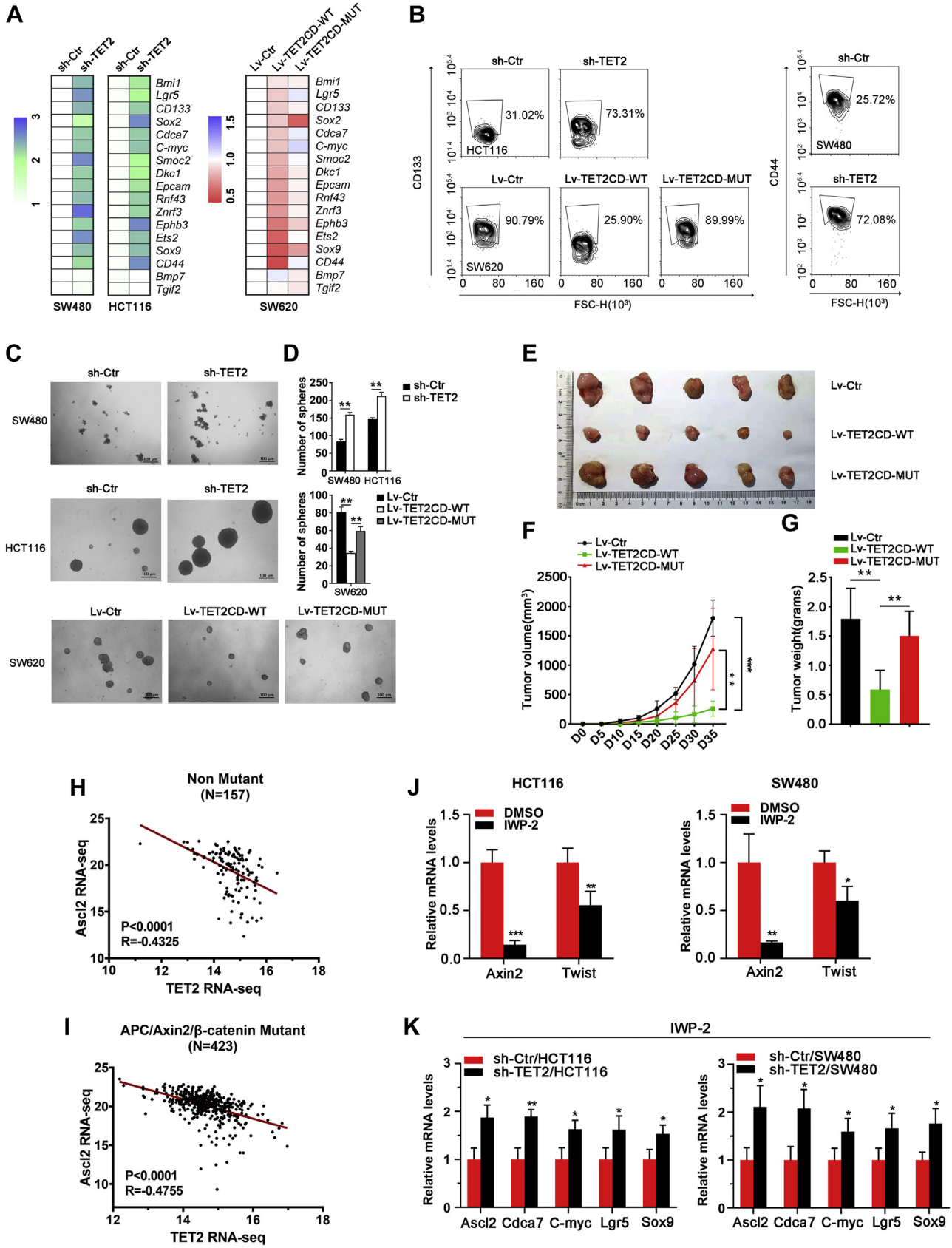

Figure 5. TET2 restrained the expression of stemness genes and the stem-like phenotypes of CRC cells. *A*, heatmap of the stemness genes displaying significant changes in stable TET2-knockdown SW480 and HCT116 cells, as well as in stable SW620 cells overexpressing the TET2-catalytic domain or mutant TET2-catalytic domain compared with their negative controls. *B*, FACS for CD133 and CD44 in the cells described in (*A*). *C*, tumorsphere cells derived from cells described in (*A*) were grown in stem cell culture media in suspension for 5 to 10 days *D*, the numbers of tumorsphere were counted from three wells

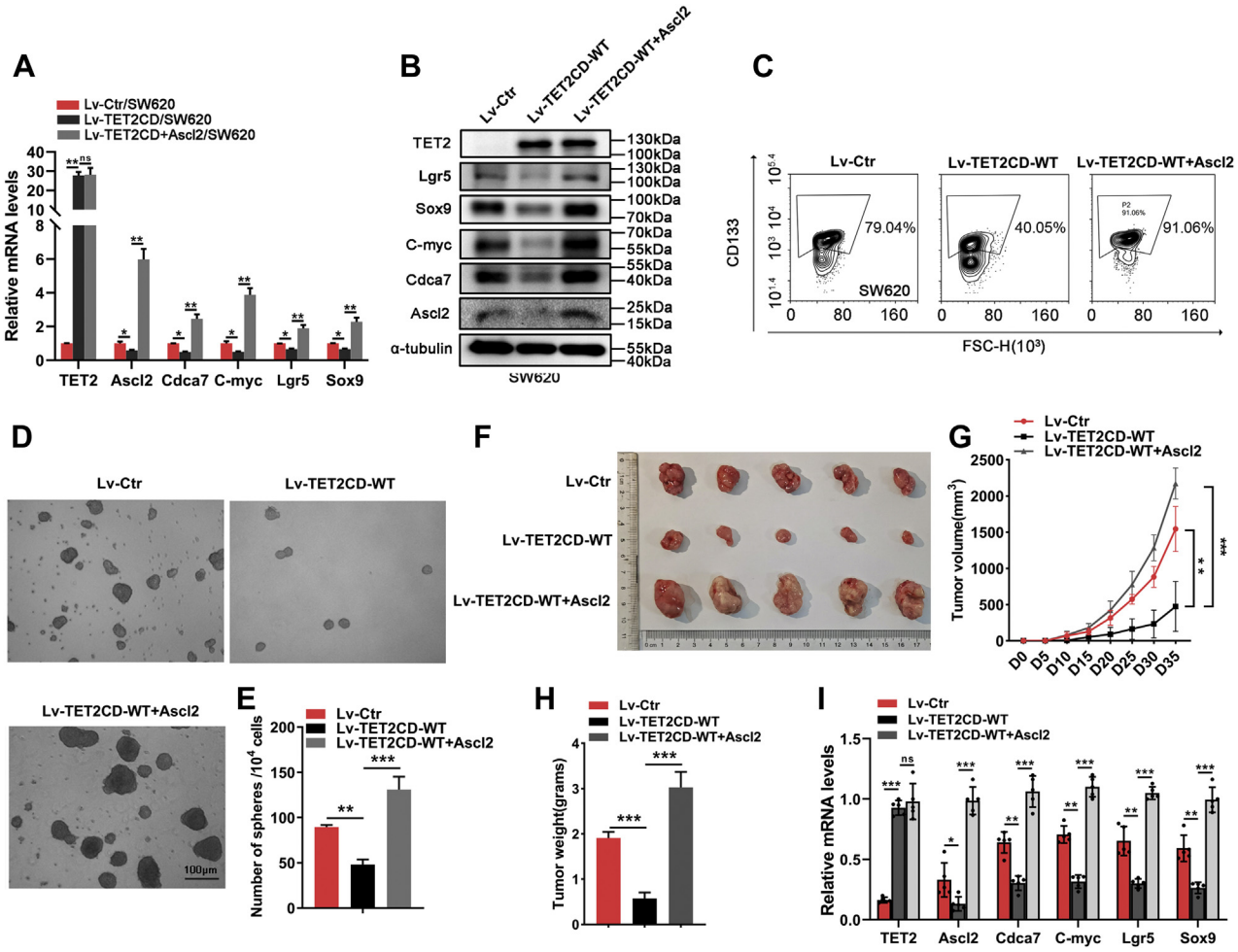

Figure 6. TET2-Ascl2 axis modulated CRC cell stemness phenotypes. *A* and *B*, the mRNA and protein expression levels of CRC cell stemness genes were detected by quantitative real-time PCR and Western blot, respectively, in stable SW620 cells overexpressing WT TET2CD (Lv-TET2CD-WT) and stable SW620 cells overexpressing WT TET2CD and heterologous Ascl2 (Lv-TET2CD-WT+Ascl2). The results are presented as mean ± SD. *C*, FACS for proportion of $CD133^+$ cells in the cells described in (*A*). *D*, tumorsphere cells derived from cells described in (*A*) were grown in stem cell culture media in suspension for 5 to 10 days *E*, the numbers of tumorsphere were counted from three wells and calculated as the mean ± SD. *F*, the *in vivo* tumorigenicity of tumorsphere cells derived from cells described in (*A*) was assessed by tumor size and weight (*F–H*). Values were mean ± SD. *I*, the mRNA levels of CRC cell stemness genes were detected by quantitative real-time PCR in tumor xenografts developed using different tumorsphere cells, n = 15. The results are presented as mean ± SD. $^{**}p < 0.01$. $^{***}p < 0.001$, unpaired two-tailed Student's *t* test. CRC, colorectal cancer; FACS, fluorescence-activated cell sorter.

counteracted the inhibition of tumorsphere formation by the WT TET2CD (Fig. 6, *D* and *E*). The *in vivo* tumorigenicity assay showed that stable SW620 cells with the WT TET2 catalytic domain had reduced tumor volume and weight compared with their control cells, while forced Ascl2 expression in stable SW620 cells with the WT TET2 catalytic domain significantly increased the tumor volume and weight (Fig. 6, *F–H*). The mRNA levels of CRC cell stemness genes in xenografts developed with different tumorspheres derived from stable SW620 cells overexpressing the WT TET2CD significantly decreased compared with control, whereas significantly increased due to Ascl2 forced expression in stable SW620 cells with WT TET2CD (Fig. 6*I*). These data suggested that TET2 regulated Ascl2 expression modulated CRC stemness phenotypes.

LC-MS/MS identified that BCLAF1 was an interactor of TET2 in CRC cells

TET2 lacks a DNA-binding domain and needs to be recruited by TFs to gene regulatory elements. LC-MS/MS identified TET2 catalytic domain–binding proteins (Table S1) that included TFs (*red*) in stable SW620 cells overexpressing the TET2 C-terminal catalytic domain (aa 1129–2002) with three FLAG epitopes at the

and calculated as the mean ± SD. *E–G*, the *in vivo* tumorigenicity of tumorsphere cells derived from stable SW620 cells overexpressing the TET2 catalytic domain or mutant TET2 catalytic domain was assessed by tumor size and weight. Values were mean ± SD. *H* and *I*, correlation analysis of TET2 and Ascl2 expression in colorectal tumors with or without activating Wnt pathway mutations (truncating mutation of APC or Axin2 or missense mutation of β-catenin) from the TCGA RNA-Seq database (n = 580). *J*, the mRNA levels of two Wnt-sensitive genes, Axin2 and Twist, were significantly inhibited in both HCT116 and SW480 cells treated with 2 mM IWP-2 for 72 h. *K*, quantitative real-time PCR for stemness genes in stable TET2-knockdown SW480 and HCT116 cells treated with 2 mM IWP-2 for 72 h. The results are presented as mean ± SD. $^{**}p < 0.01$. $^{***}p < 0.001$, unpaired two-tailed Student's *t* test. CRC, colorectal cancer; FACS, fluorescence-activated cell sorter.

N terminus, which were used for efficient immunoprecipitation. BCLAF1, as a TF (41), had the most peptides bound to the TET2 catalytic domain. Kinesin family member 11 (KIF11) was not chosen as an interactor of TET2 because it is not a TF and not involved with transcription regulation (Fig. 7*A*). Coimmunoprecipitation (Co-IP) analysis of SW620 cells transfected with the 3 × FLAG-tagged TET2 catalytic domain indicated that the TET2 catalytic domain could bind endogenous BCLAF1 (Fig. 7*B*). Stable SW620 cells overexpressing the 3 × FLAG-tagged TET2 catalytic domain were immunostained for BCLAF1 (*green*) and FLAG (*red*), and the merged image showed the overlapping *yellow* signal between BCLAF1 and FLAG in the cell nucleus stained by 4′,6-diamidino-2-phenylindole (Fig. 7*C*). The scattergram presented the overall relationship between the intensities of homologous pixels, and Pearson's correlation coefficient represented the overlap of red and green pixel intensities (Fig. 7*D*). To further confirm their interaction, we analyzed BCLAF1 interference or enforced heterologous BCLAF1 overexpression in stable SW620 cells with a 3 × FLAG-tagged TET2 catalytic domain. BCLAF1 interference led to a reduction in BCLAF1-blotting intensity but also a reduction in FLAG-blotting intensity, and BCLAF1 overexpression exerted the opposite effect (Fig. 7*E*). Finally, proximity ligation assays (PLAs) were performed to detect their interaction in stable SW620 cells with a 3× FLAG-tagged TET2 catalytic domain treated with BCLAF1 interference or enforced heterologous BCLAF1 overexpression. Quantification of PLA spots per nucleus, which provided evidence of their interaction, confirmed that BCLAF1 interference led to a significant reduction in PLA spots per nucleus and that BCLAF1 overexpression led to a significant increase in PLA spots per nucleus (Fig. 7*F*). These data provided exact confirmation that BCLAF1 was an interactor of TET2 in CRC cells.

TET2–BCLAF1 repressed Ascl2 expression by mediating hydroxymethylation and methylation levels of the Ascl2 TSS1500 promoter

To investigate the role of the TET2–BCLAF1 association in hydroxymethylation of the Ascl2 TSS1500 promoter and sequential transcription of Ascl2, we first detected the alteration of endogenous Ascl2 expression in stable SW620 cells overexpressing the TET2 catalytic domain treated with recombination plasmids expressing BCLAF1 or BCLAF1 siRNA for 72 h. The ectopic expression of BCLAF1 in stable SW620 cells overexpressing the TET2 catalytic domain strengthened the effect of TET2 on Ascl2 expression inhibition, while reduced BCLAF1 expression by siRNA almost eliminated the inhibitory effect of TET2 on Ascl2 expression (Fig. 8, *A* and *B*). The results suggested that TET2 repressed Ascl2 expression in a BCLAF1-dependent manner.

BCLAF1, as a transcription factor, contains a bZIP homolog and a Myb homolog DNA-binding motif (41). We analyzed the putative binding sites of BCLAF1 in the genome from cg01156550 to cg12499235 residing in the Ascl2 TSS1500 promoter by using the JASPAR database and found that there were three Myb-binding and five bZIP-binding sites around CCGG sites of the P1 to P4 locus (Fig. S4). These binding sites were divided into four binding regions (binding sites 1–4) according to their distance from CCGG sites, and we performed chromatin immunoprecipitation (ChIP)-qPCR analysis to determine the TET2–BCLAF1 co-occupancy on these regions by using a C-terminal antibody that recognized the TET2 catalytic domain and an antibody that recognized the hemagglutinin polypeptide conjugated to the N terminus of BCLAF1 (Fig. 8*C*) and specific primers for the detection of 5hmC and 5mC levels at CCGG sites. TET2 binding at these sites was significantly increased upon stable ectopic expression of the TET2 catalytic domain and substantially increased by the coexpression of BCLAF1, while TET2 binding at these sites was obviously decreased upon transient BCLAF1 knockdown (Fig. 8*E*).

GluMS-qPCR experiments showed that 5hmC levels at P1 to P4 were significantly increased upon BCLAF1 overexpression in stable SW620 cells with an ectopic TET2 catalytic domain compared with the control cells, which was accompanied by significant decreases in 5mC levels at the same sites (Fig. 8*D*). In contrast, even in stable TET2-overexpressing SW620 cells, BCLAF1 knockdown resulted in significant inhibition of 5hmC levels and restored 5mC levels at P1 to P4 (Fig. 8*F*). Our findings indicated that BCLAF1 could recruit TET2 to specific genomic sites at the Ascl2 TSS1500 promoter to regulate Ascl2 expression by mediating hydroxymethylation and methylation levels at the Ascl2 TSS1500 promoter.

TET2–BCLAF1 interaction counteracted stem traits of CRC cells and controlled the survival of CRC patients

To test the model in which BCLAF1 bridges TET2 to bind the Ascl2 TSS1500 promoter and thereby facilitates TET2 to regulate Ascl2 target genes, we compared transcripts associated with TET2 and BCLAF1 coexpression in CRC samples from the TCGA database by using Gene Set Enrichment Analysis (GSEA) against a gene set of mRNAs altered upon Ascl2 knockdown LS174T cells (42). Genes associated with low coexpression of TET2 and BCLAF1 were enriched for reduced transcripts upon Ascl2 knockdown (enrichment score [ES] = −0.386, normalized enrichment score [NES] = −1.468, false discovery rate (FDR) q =0.028, *p*-value = 0.031) (Fig. 9*A*), while genes associated with high coexpression of TET2 and BCLAF1 were enriched for induced transcripts upon Ascl2 knockdown (ES = 0.285, NES = 1.261, FDR q = 0.157, *p*-value = 0.160) (Fig. 9*B*). The mRNA and protein expression levels of the stem genes Cdca7, c-*myc*, Lgr5, and Sox9 in stable SW620 cells overexpressing the TET2 catalytic domain that were then transiently transfected with the BCLAF1-overexpressing construct were significantly reduced compared with their control cells but restored in stable SW620 cells overexpressing the TET2 catalytic domain that were then transiently transfected with BCLAF1-interfered siRNA for 48 h (Fig. 9, *C* and *D*). A significantly decreased proportion of $CD133^{+}$ cells in stable SW620 cells overexpressing the TET2 catalytic domain were then transiently

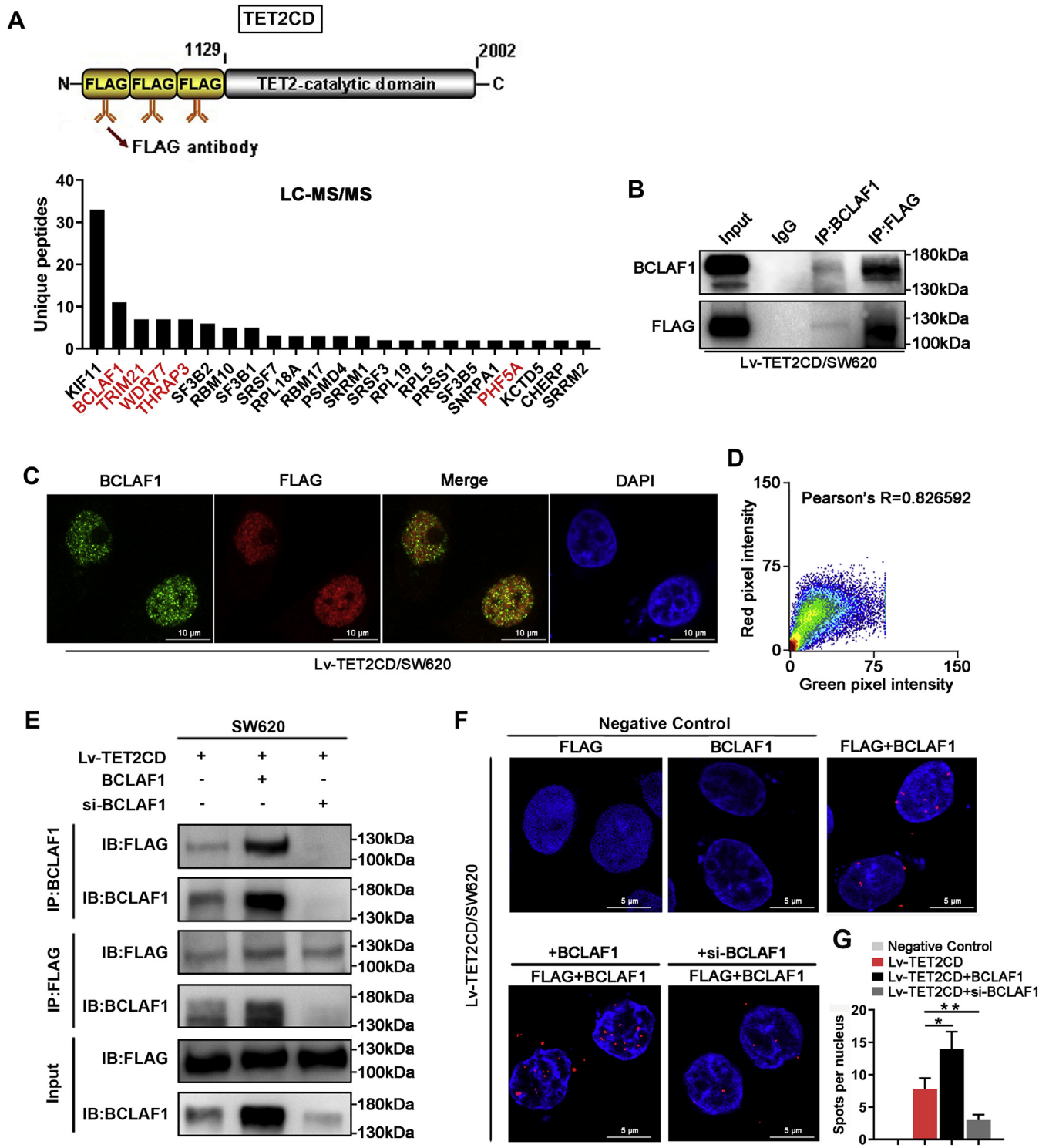

Figure 7. The TET2 catalytic domain interacted with BCLAF1 in the cellular nucleus. *A*, LC–MS/MS identified TET2 catalytic domain–binding proteins that included transcription factors (*red*) in stable SW620 cells overexpressing the TET2 C-terminal catalytic domain. Among all transcription factors, BCLAF1 had the most peptides bound to TET2 catalytic domain. *B*, Co-IP analysis of SW620 cells transfected with the 3× FLAG-tagged TET2 catalytic domain indicated that the TET2 catalytic domain could bind endogenous BCLAF1. *C*, stable SW620 cells overexpressing the 3× FLAG-tagged TET2 catalytic domain were immunostained for BCLAF1 (*green*) and FLAG (*red*). Merged images show the overlapping *yellow signal* between BCLAF1 and FLAG in the cell nucleus stained by DAPI. *D*, scattergram presenting the overall relationship between the intensities of homologous pixels. Pearson's correlation coefficient represents the overlap of *red* and *green pixel* intensities corresponding to (*C*). *E*, the TET2 catalytic domain interacted with endogenous BCLAF1 in stable SW620 cells overexpressing the 3× FLAG-tagged TET2 catalytic domain with BCLAF1 interference or with heterologous BCLAF1 overexpression. *F*, proximity ligation assays (PLAs) were performed in cells described in (*E*) to detect the interaction between the TET2 catalytic domain and BCLAF1. The negative control represents an assay with each primary antibody (FLAG or BCLAF1). *G*, quantification of PLA spots per nucleus for (*F*). PLA assays were performed in five biological replicates. The results are presented as mean ± SD. **p* < 0.05, ***p* < 0.01, ****p* < 0.001, unpaired two-tailed Student's *t* test. DAPI, 4′,6-diamidino-2-phenylindole.

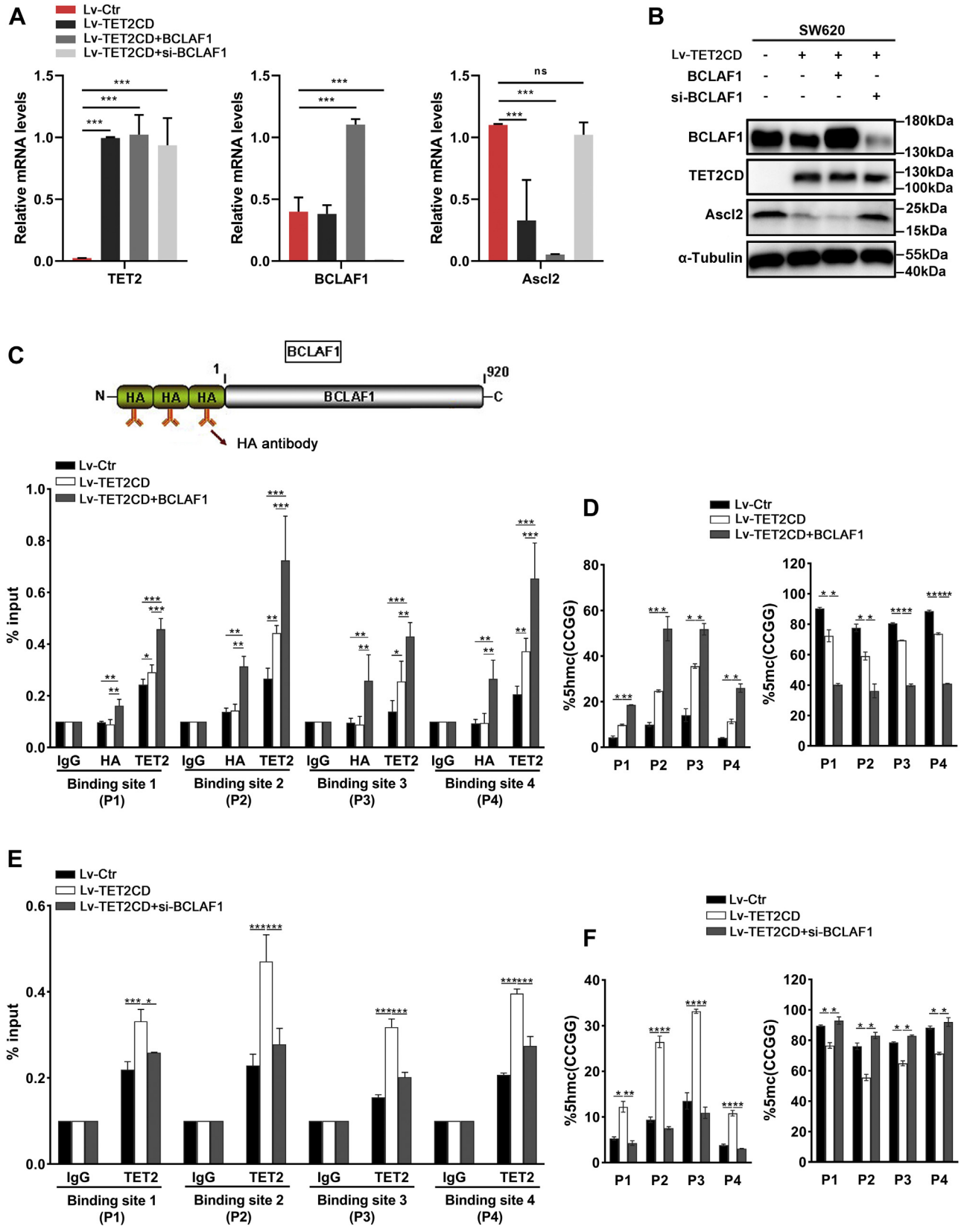

Figure 8. BCLAF1–TET2 repressed Ascl2 expression by mediating hydroxymethylation and methylation levels of the Ascl2 TSS1500 promoter. *A* and *B*, TET2, BCLAF1, and Ascl2 expression (mRNA in *A*, protein in *B*) in SW620 cells with TET2 catalytic domain overexpression or BCLAF1 overexpression or BCLAF1 interference for 48 h. *C*, stable SW620 cells transfected with lentiviral particles expressing the TET2 catalytic domain were transiently transfected with HA-BCLAF1 construct for 48 h. The occupancy of TET2 and BCLAF1 at the P1-P4 sites on the TSS1500 promoter regions of Ascl2 was determined by ChIP-qPCR with specific primers. Rabbit IgG was included as a negative control. *D*, site-specific levels of 5hmC and 5mC at TSS1500 of the Ascl2 promoter in SW620 cells described in (*C*) were determined by using GluMS-qPCR. *E*, stable SW620 cells transfected with lentiviral particles expressing the TET2 catalytic

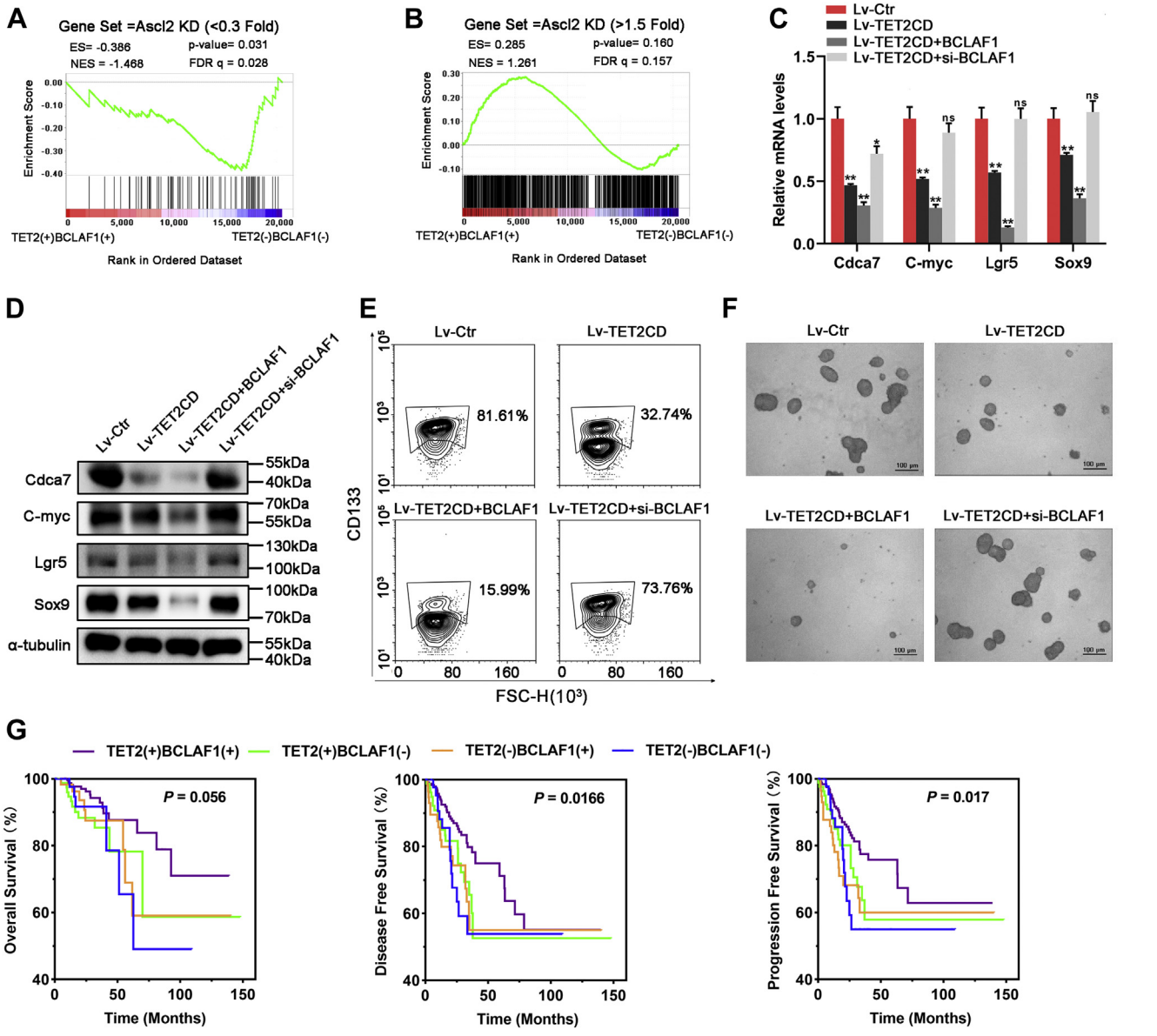

Figure 9. BCLAF1–TET2 mediated Ascl2 promoter demethylation inhibited stemness, and TET2–BCLAF1 coexpression patterns predicted CRC patient survival. *A* and *B*, GSEA of the downstream genes of Ascl2 (Oikonomou *et al. cell reports*. 2015) between CRC patients with *high* coexpression of TET2 and BCLAF1 *versus* those with *low* coexpression of TET2 and BCLAF1. *C* and *D*, the mRNA and protein expression levels of Cdca7, c-*myc*, Lgr5, and Sox9 in stable SW620 cells overexpressing the TET2 catalytic domain, which were then transiently transfected with a BCLAF1-overexpressing construct or BCLAF1-interfered siRNA for 48 h *E*, FACS for CD133 in stable SW620 cells described as (*C* and *D*). *F*, tumorsphere cells were derived from stable SW620 cells described as (*C* and *D*), and spheres were formed on the fifth day after transfection. *G*, survival analysis of 444 CRC patients with coexpression of TET2 and BCLAF1. $*p < 0.05$, $**p < 0.01$, unpaired two-tailed Student's *t* test. CRC, colorectal cancer; FACS, fluorescence-activated cell sorter.

transfected with the BCLAF1-overexpressing construct (15.99%) compared with SW620 cells (81.61%) and stable SW620 cells overexpressing the TET2 catalytic domain (32.74%) but were restored in stable SW620 cells overexpressing the TET2 catalytic domain, which were then transiently transfected with BCLAF1-interfered siRNA (73.76%) (Fig. 9*E*). Tumorsphere cells were derived from SW620 cells with overexpression of both the TET2 catalytic domain and BCLAF1, and spheres were formed on the fifth day after transfection. The tumorsphere formation potential was inhibited in SW620 cells overexpressing both the TET2 catalytic domain and BCLAF1 and recovered in stable SW620 cells overexpressing the TET2 catalytic domain, which were then transiently transfected with BCLAF1 siRNA (Fig. 9*F*).

Survival analysis of 444 CRC patients according to TET2 and BCLAF1 expression levels was performed using the

domain were transfected with BCLAF1-interfered siRNA for 48 h. The occupancy of TET2 at P1-P4 sites on the TSS1500 promoter regions of Ascl2 was determined by ChIP-qPCR with specific primers. Rabbit IgG was included as a negative control. *F*, site-specific levels of 5hmC and 5mC at TSS1500 of the Ascl2 promoter in SW620 cells described in (*E*) were determined by using GluMS-qPCR. $^{ns}p > 0.05$, $*p < 0.05$, $**p < 0.01$. $***p < 0.001$, unpaired two-tailed Student's *t* test. ChIP, chromatin immunoprecipitation; GluMS, glucosylated hydroxymethyl–sensitive; qPCR, quatitative PCR; TSS, transcription start site.

Kaplan–Meier survival analysis method. Patients were divided further into four groups based on the expression levels of TET2 and BCLAF1: TET2 (+) BCLAF1 (+), TET2 (+) BCLAF1 (–), TET2 (–) BCLAF1 (+), and TET2 (–) BCLAF1 (–). TET2–BCLAF1 mRNA expression levels were associated with patient OS (p = 0.056), DFS (p = 0.0166), and progression-free survival (p = 0.017) (Fig. 9*G*). The results suggested that these two genes may be used as prognostic markers for patients according to their associated expression levels.

Discussion

Our study provides an epigenetically important delineation of how TET2 drives Ascl2 promoter hydroxymethylation and demethylation through recruitment by BCLAF1 to the Ascl2 TSS1500 promoter and how this contributes to key Ascl2-dependent malignant properties of CRC. First, there are implications regarding the interplay between TSS1500 promoter hypermethylation, CRC biology, prognosis of CRC patients, and the balance of roles for critical TET2–BCLAF1 interaction and their specific binding to Ascl2 TSS1500 promoter in its hypermethylation maintenance *via* TET2–BCLAF1–mediated demethylation remodeling. For methylation maintenance of the Ascl2 TSS1500 promoter, our data demonstrated that there is an absolute requirement of TET2 and BCLAF1, which mediate recognition of the potential three Myb-binding and five bZIP-binding sites around CCGG sites, respectively. These distinctions suggest that targeting the TET2–BCLAF1 complex may hold therapeutic potential for preventing Ascl2 TSS1500 promoter remethylation after demethylating activity.

CRC is the third leading cause of death from cancer worldwide (43). Cancer stem cells, a subpopulation of cancer cells, have been proposed to explain the functional heterogeneity and carcinogenesis of cancer (44, 45). It is important to identify the regulatory mechanisms and signaling pathways involved in CRC progenitor cells to develop novel reagents to target the refractory CRC progenitor cell population (45). Ascl2 can be regulated by the hpo/Mst signaling pathway, as well as the Tssc3, HIF 1α and 2α, L1 family of cell adhesion receptors, and through Ascl2 autoregulation (9, 46–50). Although it was reported that aberrant upregulation of Ascl2 by promoter demethylation promotes the growth and resistance to 5-fluorouracil of gastric cancer cells (51), there is no available report about the epigenetic regulatory mechanism regulating abnormal expression of Ascl2 in CRC cells. DNA methylation is one of the most important hallmarks of tumor development and progression. While the role of hypermethylation in the silencing of tumor suppressor genes is well documented, DNA methylation is also a dynamic epigenetic indicator that undergoes extensive changes during the differentiation of self-renewing stem cells and is responsible for the regulation of the expression of some stem cell markers, such as CD133, OCT4, and NANOG (52). We found that Ascl2 TSS1500 promoter (-1670–-1139) hypermethylation was an epigenetic switch to activate Ascl2 expression.

In cancer, global patterns of DNA methylation are altered with global hypomethylation of repeat-rich intergenic regions and hypermethylation of a subset of CpG-dense gene-associated regions (CpG islands). The classical model of DNA methylation is recognized in gene silencing and strong evidence supports this paradigm. The prominent gene-silencing role of human DNA methylation is now being questioned in particular biological contexts, including carcinogenesis, metastasis, development, and induced pluripotent stem cells (16). Aberrant DNA methylation in promoters leads to inappropriate transcriptional activation of some oncogenes (53). Failure to demethylate and to consequently reactivate these methylation-induced tumor genes is a contributor to tumor progression. One of the possible reasons for the failure to demethylate these methylated genes is the deregulation of the TET pathway (54). 5hmC is considered an intermediate in an active demethylation process catalyzed by the TET family, which comprises three members, TET1 to TET3, that have combinatory roles in different developmental processes as well as carcinogenesis (54). The decrease in TETs and 5hmC was identified as a hallmark of multiple types of solid tumors, and importantly, enhanced expression of TET2 suppresses both the proliferation and metastasis of cancer cells (55, 56). TET2 is a unique member of this family that is highly expressed in hematopoietic lineages. Several recent studies have shown that the level of 5hmC in many various types of human malignancies, including CRC, is profoundly reduced and that the degree of the reduction is proportional to tumor stage (57). The Ascl2 TSS1500 promoter (–1670–-1139) had CpG-dense gene-associated regions and had hypermethylation levels that were regulated by TET2 expression in CRC cells. TET2 downregulation in CRC cells led to dysfunction of demethylation and further led to Ascl2 TSS1500 promoter (–1670–-1139) hypermethylation and Ascl2 overexpression.

However, TET2 lacks the CXXC DNA-binding domain, which is present in TET1 and TET3 (58). It is unclear how TET2 binds to a specific locus in the genome, and direct TET2 binding at promoters or enhancers of target genes within cells has not been reported. Immunopurification coupled with mass spectrometry (IP–LC-MS/MS) has been previously used by a number of groups in attempts to identify TET-interacting proteins. By this approach, a few proteins have been identified and functionally characterized, including O-linked β-N-acetylglucosamine transferase (OGT) (59). Our IP–LC-MS/MS experiment identified that BCLAF1 was an interactor of TET2 in CRC cells. BCLAF1 is involved in diverse biological processes, including apoptotic signaling, posttranscriptional processes, Kaposi's sarcoma-associated herpesvirus and human cytomegalovirus infection, lung development, T-cell activation, angiogenesis, and carcinogenesis (60–62). BCLAF1 regulates the tumorigenesis of colon cancer cells (60), and the prominent features of the BCLAF1 structure are the bZIP and Myb DNA-binding domains, which are essential for BCLAF1 function in transcriptional regulation (41). Our present results confirmed that BCLAF1 bound to bZIPs and that Myb resided at the Ascl2 TSS1500 promoter, recruiting TET2 and leading to TET2–BCLAF1–mediated demethylation reprogramming, further relative hypomethylation, and finally Ascl2 transcriptional suppression.

In summary, this study described Ascl2 TSS1500 promoter hypermethylation due to TET2–BCLAF1–mediated demethylation remodeling functioning as an additional and novel Ascl2-upregulating mechanism in CRC cells and further conferred to Ascl2-dependent CRC cell fate (Fig. 10). Our work served as the basis for the possible design of targeted therapy to enhance TET2–BCLAF1 function, reverse Ascl2 TSS1500 promoter methylation status, and control Ascl2-dependent maintenance of the stemness of cancer stem cells in CRC tissues.

Experimental procedures

Human specimens

Patients with CRC who were scheduled for colonoscopy at Southwest Hospital and 958 Hospital, Third Military Medical University were enrolled in the study. Fresh CRC specimens and matched adjacent tissues were collected from 17 CRC patients by biopsy and immediately stored in liquid nitrogen for further quantitation of Ascl2 mRNA and 5hmC as well as 5mC levels of Ascl2 TSS1500 promoter. The study was approved by the local ethics committee. All provided informed consent or resection surgery. Informed consent for the study was signed by all of the subjects before their colonoscopy.

Sequences of the oligonucleotides and antibodies

Sequences of the oligonucleotides used for real-time PCR, ChIP-qPCR, siRNA, and shRNA was shown in Table 1, and the antibodies used Western blotting, flow cytometry analysis, immunofluorescence, ChIP assay, Co-IP, and PLA were shown in Table 2.

Cell lines

The LOVO, HCT116, SW480, and SW620 human colonic adenocarcinoma cell lines were obtained from Chinese Academy of Sciences Cell Bank of Type Culture Collection. All aforementioned cells were cultured in Dulbecco's modified Eagle's medium (DMEM) medium with fetal bovine serum at 10% v/v and maintained at 37 °C with 5% CO_2.

Bioinformatics analysis

TCGA colorectal adenocarcinoma DNA methylation data across genome regions of Ascl2 (TSS1500, TSS200, 5′-UTR, first exon, and 3′-UTR) was obtained from MethHC database. The β-value of Ascl2 in colorectal adenocarcinoma primary tumors and their adjacent normal tissues were compared by Student's *t* test. To define DMCs associated to Ascl2 mRNA level, we first downloaded methylation data of the CpG probes and transcript data of Ascl2 from Mexpress database to analyze the correlation between them. The genomic locations of these methylated CpGs, which were significantly associated with Ascl2 mRNA level ($p < 0.05$), and their methylated status in Caco2 colon cancer cells were visualized by UCSC Genome Browser. Next, we compared the methylation levels of these CpG sites in primary tumor tissues from CRC patients and their adjacent normal tissues and screened out the significantly DMCs. For survival analysis and Cox

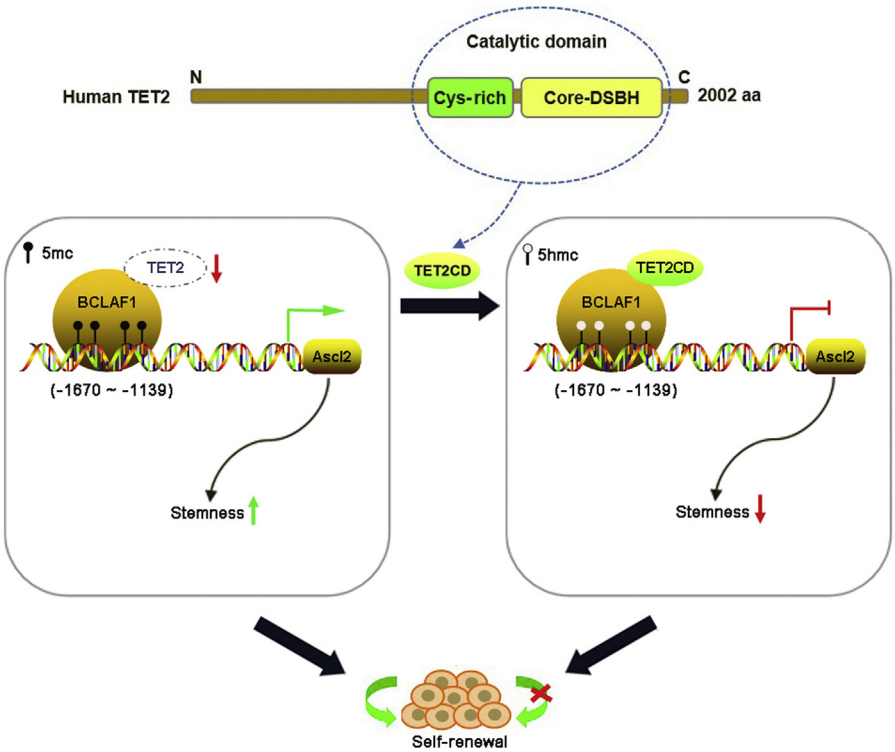

Figure 10. Our proposed hypothesis detailing the epigenetic remodeling within the Ascl2 promoter by TET2–BCLAF1 modulates colorectal cancer cell stemness.

Table 1
Sequences of the oligonucleotides used for qPCR, ChIP-qPCR, siRNA, and shRNA

Type	Sequence
Primers for qPCR	**5′-3′**
TET2	F: AGACTATGTGCCTCAGAAATCC
	R: CCCTGTGACCCGAGTGAA
BCLAF1	F: TCTGGAATAGAAGGCACTCTAGG
	R: ACCCTCGTCTTTTAGAAACAGGA
α-tubulin	F: ACCTTAACCGCCTTATTAGCCA
	R: ACATTCAGGGCTCCATCAAATC
Ascl2	F: CGTGAAGCTGGTGAACTTGG
	R: GGATGTACTCCACGGCTGAG
Cdca7	F: CTCCTAATTTCTTCTGCCCGAA
	R:ATTACATTGCCCACCAACCTTT
C-myc	F: GGCTCCTGGCAAAAGGTCA
	R: CTGCGTAGTTGTGCTGATGT
Lgr5	F: CTGCCTGCAATCTACAAGGT
	R: CCCTTGGGAATGTATGTCAGA
Sox9	F: CTCTGGAGACTTCTGAACGA
	R: ACTTGTAATCCGGGTGGTC
Bmi1	F: AAATGCTGGAGAACTGGAAAG
	R: CTGTGGATGAGGAGACTGC
CD133	F: GCCACCGCTCTAGATACTGC
	R: TGTTGTGATGGGCTTGTCAT
CD44	F: AGCAACCAAGAGGCAAGAAA
	R:GTGTGGTTGAAATGGTGCTG
Sox2	F: TACAGCATGTCCTACTCGCAG
	R: GAGGAAGAGGTAACCACAGGG
Smoc2	F: AAGGAAGTATACCCAGGAGCAA
	R: GTGTAGCTGTGACACTGGACCT
Dkc1	F: GGTATAGTAGCCAAGATCAAGAG
	R: TTCTGACTTGCCTTTGGAC
Rnf43	F: ATCACTGAGGATCGAGCTG
	R: CTTCTCAGCGTCATTACCC
Znrf3	F: GCTATTGATCAGCTGAACCAG
	R: CTTAATGGCATCTGCACCC
Ephb3	F: GTTTGAGACCACAAGTGAGAG
	R: ATAGCGATGACCACGACAG
Ets2	F: ATTCCATTTCTCATGACTCCG
	R: TTAAGGCTTGACTCATCACAG
Axin2	F: CAACACCAGGCGGAACGAA
	R: GCCCAATAAGGAGTGTAAGGACT
Twist	F: GTCCGCAGTCTTACGAGGAG
	R: GCTTGAGGGTCTGAATCTTGCT
Bmp7	F: TCGGCACCCATGTTCATGC
	R: GAGGAAATGGCTATCTTGCAGG
Tgif2	F: TGACCCCTGGTAGCACACTTA
	R: GTGGTGGCGTGTTGAAGAGT
Primers for 5hmc/5mc-specific PCR	**5′-3′**
P1	F: AACCCGCCCCGCTTTCC
	R: AAGGTGCCGCCCAGAGCC
P2	F: CTCTGGGCGGCACCTTA
	R: GGAAGCGAGACGGAGAACA
P3	F: CTTGGCAAAGGCTCCC
	R: TTAGGTCCTGCCTCACTG
P4	F: GGGGGAGCCTTTGCCA
	R: AAATCTCCGTTCCCTGAGGT
siRNA and shRNA for TET2	**5′-3′**
siRNA-496	GGAUAGAACCAACCAUGUUTT
	AACAUGGUUGGUUCUAUCCTT
siRNA-1417	GCUAAAUACCUGUUCCUUUTT
	AAAGGAACAGGUAUUUAGCTT
siRNA-2077	GCAGUUGAUGAGAAACAAATT
	UUUGUUUCUCAUCAACUGCTT
shRNA for TET2	GCTAAATACCTGTTCCTTT
siRNA for BCLAF1	**5′-3′**
siRNA-956	CCACCUAGUCAGAGUUCAUTT
	AUGAACUCUGACUAGGUGGTT
siRNA-1229	GGAGAUCAGGAAACUGCAATT
	UUGCAGUUUCCUGAUCUCCTT
siRNA-1967	GCUAGUACACUUGUCCAUUTT
	AAUGGACAAGUGUACUAGCTT

Primers for ChIP-qPCR were consistent with primers for 5hmc/5mc-specific PCR.
Abbreviations: F, forward; R, reverse.

regression analysis, clinical data of CRC patients from TCGA were downloaded from the Cbioportal website (http://www.cbioportal.org).

For GSEA analysis, a gene set (NCBI GEO: GSE69036) consisting of 1144 transcripts upregulated > 1.5-fold and 47 transcripts downregulated < 0.3-fold in Ascl2-knockdowned LS174T colon cancer cells was used to compare with a ranked list of 20,521 transcripts sorted from high coexpression of TET2 and BCLAF1 TCGA dataset, relative to low coexpression of TET2 and BCLAF1 TCGA dataset. The transcriptome data of CRC patients from TCGA was downloaded from the Cbioportal website.

Inhibition and induction of TET2 activity by DMOG, DFO, and vitamin C

DMOG and DFO (Sigma–Aldrich) were used to inhibit TET2 activity with 500 μm in SW480 cells for 0, 2, 4, and 8 h. Vitamin C (Sigma–Aldrich) was used to induce TET2 activity with 500 μg/ml in SW620 cells for 0, 2, 4, and 8 h and with 0, 100, 500, and 1000 μg/ml in SW620-derived tumorsphere cells for 5 days.

Cell lentiviral infection and transfection

HCT116 and SW480 cells were infected with TET2 shRNA lentiviral (GenePharma Co Ltd) (Table 1). SW620 cells were infected with lentiviral particles expressing 3× FLAG-tagged TET2 WT or TET2 mutant catalytic domain (Tsingke Co Ltd). Stable cells with TET2 knockdown or TET2 ectopic expression were established by selecting infected cells with puromycin for 2 weeks. Stable HCT116 and SW480 cells with TET2 knockdown were infected with lentiviral particles expressing 3× FLAG-tagged TET2 WT or TET2 mutant catalytic domain.

Stable SW620 cells with TET2 WT catalytic domain were transfected with 2 μg pcDNA3.1 plasmid containing Ascl2 or 3× HA-tagged BCLAF1 encoding sequence (Tsingke Co Ltd) by using the X-tremeGENE HP transfection reagent (Roche) or transfected with 150pmol BCLAF1 siRNA (GenePharma Co Ltd), using the GP-transfect-Mate transfection reagent (GenePharma Co Ltd). The cells were harvested 48 h after transfection or selected using G418 (800 mg/ml) for 2 weeks.

Inhibiting Wnt signaling assay

HCT116 and SW480 cells and their stable cells with TET2 knockdown were seeded in 6-well plates and treated with 2 μM IWP-2 (GlpBio). Cells were collected at 72 h and used for RNA extraction and real-time PCR for Axin2, Twist, Ascl2, Lgr5, Cdca7, c-*myc*, and Sox9 mRNA detection.

Flow cytometry analysis

For the analysis of $CD133^+$ or $CD44^+$ cell populations, the single cell suspension was detached using 0.02% EDTA in PBS, counted, and washed in PBS. At least 10^6 cells were incubated with APC Mouse anti-CD133 antibody or APC-H7 Mouse anti-CD44 antibody (Table 2) at 4 °C for 20 min in the dark, as well as their negative control. After the washing steps, the labeled cells were analyzed with a fluorescence-activated cell sorter (BD Biosciences).

Table 2
Antibodies used in this study

Antibodies	Source	Identifier
Mouse monoclonal anti-TET2 (clone hT2H 21F11), N-terminus	Millipore	Cat# MABE462
Rabbit monoclonal anti-TET2, C-terminus	Cell Signaling	Cat# 18950S
Rabbit polyclonal anti-BTF (clone EPR18803)	Bethyl	Cat# A300-610A
Mouse monoclonal anti-Ascl2 (clone 7E2)	Millipore	Cat# MAB4418
Mouse monoclonal anti-FLAG (clone M2)	Sigma–Aldrich	Cat# F3165
Rabbit monoclonal anti-HA (C29F4)	Cell Signaling	Cat#3724
Normal Rabbit IgG control	Cell Signaling	Cat#2729
Rabbit polyclonal anti-LGR5	Bioworld Technology	Cat# BS72291
Rabbit polyclonal anti-SOX9	Bioworld Technology	Cat#BS91275
Rabbit polyclonal anti-CDCA7	Proteintech	Cat#15249-1-AP
Rabbit polyclonal anti-c-MYC	Proteintech	Cat#10828-1-AP
Rabbit polyclonal anti-α-tubulin	Proteintech	Cat#11224-1-AP
APC Mouse anti-CD133 (clone W6B3C1)	BD Biosciences	Cat# 566596
APC-H7 Mouse anti-CD44 (clone G44-26)	BD Biosciences	Cat# 560532
APC Mouse IgG1 κ Isotype Control (clone MOPC-21)	BD Biosciences	Cat# 554681
APC-H7 Mouse IgG2b, κ Isotype Control (clone 27-35)	BD Biosciences	Cat# 560183

Abbreviations: Cat, catalog.

Tumorsphere formation and mouse xenografts assays

For tumorsphere formation assay, single cell suspensions were plated on 6-well ultralow attachment plates (Costar) at a density of 10^4 cells/ml. Colon tumorsphere cells were grown in a serum-free DMEM/F12 medium (Hyclone) supplemented with B27 (Invitrogen), 20 ng/ml EGF (STEMCELL), 20 ng/ml bFGF (STEMCELL), and 4 μg/ml heparin (STEMCELL) for 7 days. The numbers of the spheres were quantified by using an inverted microscope (Olympus) at 100× magnification.

For mouse xenografts assay, 10^4 suspended cells from tumorsphere were mixed with Matrigel matrix (Corning) in a volume ratio of seven to three and injected subcutaneously into the flank area of 5-week-old male nude mice (GemPharmatech) with 100 μl volume. After 35 days, the nude mice were sacrificed and their tumor weight and size were measured.

LC-MS/MS analysis

The 10^8 stable SW620 cells with ectopically expressing 3× FLAG tagged TET2 WT catalytic domain were scraped and then lysed with IP lysis (Thermo Fisher Scientific) at 4 °C. The supernatant of lysed cells was subjected to immunoprecipitation with 3 μg anti-FLAG antibody or IgG antibody (Table 2) overnight at 4 °C. The 25 μl protein A/G Magnetic beads (Thermo Fisher Scientific) prewashed with IP lysis twice were added and incubated with the antigen sample/antibody mixture for 1 h at room temperature (RT) with mixing. Protein complex–containing beads were washed with IP lysis four times and eluted with low-pH elution buffer (Thermo Fisher Scientific) to obtain the supernatant containing the target antigen immunized with anti-FLAG antibody.

Filter-aided sample preparation (FASP Digestion): 200 μg of proteins for each sample were incorporated into 30 μl SDT buffer (4% SDS, 100 mM DTT, 150 mM Tris–HCl pH 8.0). The detergent, DTT, and other low-molecular weight components were removed using UA buffer (8 M urea, 150 mM Tris–HCl pH 8.0) by repeated ultrafiltration (Microcon units, 10 kD). Then 100 μl iodoacetamide (100 mM IAA in UA buffer) was added to block reduced cysteine residues, and the samples were incubated for 30 min in darkness. The filters were washed with 100 μl UA buffer three times and then 100 μl 25 mM NH_4HCO_3 buffer twice. Finally, the protein suspensions were digested with 4 μg trypsin (Promega) in 40 μl 25 mM NH_4HCO_3 buffer overnight at 37 °C, and the resulting peptides were collected as a filtrate. The peptides of each sample were desalted on C18 Cartridges (Empore SPE Cartridges C18 (standard density), bed I.D. 7 mm, volume 3 ml, Sigma), concentrated by vacuum centrifugation, and reconstituted in 40 μl of 0.1% (v/v) formic acid. The peptide content was estimated by UV light spectral density at 280 nm using an extinctions coefficient of 1.1 of 0.1% (g/l) solution that was calculated on the basis of the frequency of tryptophan and tyrosine in vertebrate proteins.

HPLC: Each fraction was injected for nanoLC-MS/MS analysis. The peptide mixture was loaded onto a reverse phase trap column (Thermo Scientific Acclaim PepMap100, 100 μm*2 cm, nanoViper C18) connected to the C18-reversed phase analytical column (Thermo Scientific Easy Column, 10 cm long, 75 μm inner diameter, 3 μm resin) in buffer A (0.1% formic acid) and separated with a linear gradient of buffer B (84% acetonitrile and 0.1% formic acid) at a flow rate of 300 nl/min controlled by IntelliFlow technology. The linear gradient was determined by the project proposal: 1 h gradient: 0 to 60% buffer B for 50 min, 60 to 90% buffer B for 4 min, hold in 90% buffer B for 6 min.

LC-MS/MS analysis: LC-MS/MS analysis was performed by using a Q Exactive mass spectrometer connected to Easy-nLC 1000 UHPLC system (Proxeon Biosystems, now Thermo Fisher Scientific) at Shanghai Applied Protein Technology Co Ltd in China. The mass spectrometer was operated in positive ion mode. MS data were acquired using a data-dependent top10 method dynamically choosing the most abundant precursor ions from the survey scan (300–1800 m/z) for higher-energy collisional dissociation fragmentation. Automatic gain control target was set to 1e6, maximum inject time to 40 ms , and number of scan ranges to 1. Dynamic exclusion duration was 30.0 s. Survey scans were acquired at a resolution of 70,000 at m/z 200 and resolution for higher-energy collisional dissociation spectra was set to 17,500 at m/z 200, isolation width was 2 m/z,

microscans to 1, and maximum inject time to 50 ms. Normalized collision energy was 27 eV and the underfill ratio, which specifies the minimum percentage of the target value likely to be reached at maximum fill time, was defined as 0.1%. The instrument was run with peptide recognition mode enabled. The raw MS data were searched against the Uniprot human protein database (https://www.uniprot.org/), which contains 18,843 sequences as of February 17, 2020 by using the Mascot algorithm (Xcalibur3.1, version 2.2, Matrix Science) with the following parameters: mass tolerance for precursor ions = 20 ppm, mass tolerance for precursor ions = 0.1 Da, enzyme to generate peptides = trypsin, filter by peptide confidence = high (FDR < 0.01), FDR = 2× Ndecoy(t)/(Ndecoy(t)+Nnormal(t)), Ndecoy(t): actual number of false positives (FP) from decoy database, Nnormal(t): actual number of true positives (TP) from target database. Variable modification: Oxidation (M); Fixed modification: Carbamidomethyl (C); Missed cleavage = 2.

Immunofluorescence colocalization

For immunofluorescence colocalization analysis, cells grown on 24 mm glass coverslips, were fixed in 4% paraformaldehyde for 30 min at RT, and permeabilized with 0.5% Triton X-100. After blocking with 2.5% bovine serum albumin in PBS (blocking solution) for 1 h, the cells were incubated with rabbit polyclonal anti-BCLAF1 (1:1000) and mouse monoclonal anti-FLAG (1:1000) diluted in blocking solution overnight at 4 °C. The cells were washed three times with PBS and incubated with 50 μl Alexa Fluor 488-conjugate (anti-rabbit, 1:1000) and Alexa Fluor 594-conjugated (antimouse, 1:1000) secondary antibodies (Cell Signaling) at RT for 30 min in the dark. Monolayers were washed with PBS, and cell nuclei were stained with 50 μl 4′,6-diamidino-2-phenylindole (Sigma–Aldrich) solution for 10 min at RT. The analysis of immunofluorescence was performed with a Zeiss LSM 780 confocal laser scanner microscope (Carl Zeiss) equipped with a 100× oil objective and ZEN lite 2.0 software (ZEISS). Colocalization Finder, a plugin in ImageJ software was used to analyze the overall relationship between red and green pixel intensities.

Duolink PLA

PLA was performed using the Duolink *In Situ* Red Starter Kit (Sigma–Aldrich) following the manufacturer's instructions. Cells were fixed in 4% paraformaldehyde for 30 min at RT and then permeabilized with 0.2% Triton X-100 (v/v in PBS) for 20 min at RT. After blocking with Duolink Blocking Solution in a heated humidity chamber for 1 h at 37 °C, cells were incubated overnight at 4 °C with primary antibodies specific for FLAG (Sigma–Aldrich) and BCLAF1 (Bethyl) in diluent buffer. PLA oligonucleotide probes incubated for 1 h at 37 °C with samples to hybridize and then ligated together with a ligation-ligase solution for 30 min at 37 °C. After rolling circle amplification for 100 min at 37 °C, each interaction generated a fluorescent spot that was analyzed under a Zeiss LSM 780 confocal laser scanner microscope (Carl Zeiss) equipped with a 100× oil objective and ZEN lite 2.0 software. Negative control was performed with one primary antibody alone. Protein–protein interactions appeared as red spots. Images were processed and red dots counted using the ImageJ software.

Co-IP

Stable SW620 cells with ectopically expressing TET2 WT catalytic domain upon BCLAF1 overexpression or BCLAF1 interference were lysed using Magnetic IP/Co-IP Kit (Thermo Fisher Scientific) according to the manufacturer's protocol. The cell lysates were incubated with 3 μg anti-FLAG antibody, anti-BCLAF1 antibody, or IgG antibody (Table 2) overnight at 4 °C, and the mixture was then incubated with protein A/G magnetic beads for 1 h at RT. After thorough washing four times, the protein samples were eluted with SDS-PAGE 5× loading buffer containing 50 nm DTT (Beyotime Biotechnology) for 15 min at RT and then processed on 6% SDS-PAGE gels and analyzed by Western blot.

Western blot assay

Cell lysates dissolved in SDS sample buffer were separated by SDS-PAGE and transferred to a polyvinylidene difluoride membrane (Millipore). The membrane was probed with primary antibody overnight at 4 °C. Primary antibodies used in Western blot were shown in Table 2. α-Tubulin was used as a control. Detailed Western blotting procedures have been described previously (7). The band intensity was analyzed using ImageJ. The densitometric data were compared with the α-tubulin band intensity of respective samples.

RNA isolation and real-time PCR analysis

Total RNA was isolated from the cells using Eastep Super Total RNA Extraction Kit (Promega). Complementary DNA was synthesized by using the PrimeScript RT reagent kit (TaKaRa). Real-time PCR was performed with the SYBR premix Ex TaqTM Green II (TaKaRa). Relative expression levels were normalized to the expression level of α-tubulin and calculated by the formula $2^{-\Delta\Delta Ct}$ using CFX Manager software (Bio-Rad). The primers used for PCR amplification were shown in Table 1.

ChIP-qPCR assays

For ChIP-qPCR assays, the detailed procedure was referred to the SimpleChIP Enzymatic Chromatin IP Kit (Cell Signaling). Briefly, 2×10^7 cells were crosslinked with 1% formaldehyde in medium at RT for 10 min. Total cell lysates containing chromatin were digested by micrococcal nuclease to generated 150 to 900 bp DNA fragments at 37 °C for 20 min. Chromatin was immunoprecipitated with anti-TET2 (Cell Signaling), anti-FLAG (Sigma–Aldrich), and anti-HA (Cell Signaling). All resulting precipitated DNA samples were quantified by real-time PCR. Data are calculated as the percentage of input DNA referring to the formula input% = 2% × $2^{(Ct\ 2\%\ input\text{-}Ct\ IP\ samples)}$. The primer sequences used for qPCR were as listed in Table 1.

GluMS-qPCR analysis

Locus-specific 5hmC and 5mC levels in DMCs were measured using the EpiMark 5hmC and 5mC Analysis Kit

(New England Biolabs) according to the manufacturer's instructions. Briefly, 5 μg genomic DNA from cells or tissues was treated with or without T4 β-glucosyltransferase (T4-BGT) (30 units) for 16 h at 37 °C, which could add a glucose moeity to 5hmC to generate the glucosylated 5hmC (5-ghmC). The glucosylated or nonglucosylated DNA was then digested with 100 units MspI or 50 units HpaII or without enzyme at 37 °C for 12 h. MspI will cleave CCGG sites modified with 5mC and 5hmC but not 5-ghmC. Whereas, HpaII will cleave only completely unmodified CCGG sites: any modification (5mC, 5hmC, or 5-ghmC) at either cytosine blocks cleavage. Based on the aforementioned principles, the samples were divided into six different treatment groups, as shown here: tube 1: DNA + T4-BGT + UDP-Glc + MspI, tube2: DNA + T4-BGT + UDP-Glc + HpaII, tube 3: DNA + T4-BGT + UDP-Glc, tube 4: DNA + UDP-Glc + MspI, tube 5: DNA + UDP-Glc + HpaII, tube 6: DNA + UDP-Glc. Each digested sample was incubated with 1 μl proteinase K and 40 °C for 30 min and inactivated proteinase K by incubating at 95 °C for 10 min. Real-time PCR was then performed on 1 μl final DNA product using site-specific primers (Table 1) and the Ct values represented the amounts of cleaved and uncleaved amplicons containing CCGG sites. For the convenience of comparison, real-time PCR data were normalized to the nonglucosylated/undigested DNA sample (tube 6) based on $2^{-\Delta\Delta Ct}$ formula. And, the normalized Ct values were used to calculate the percentage of 5mC and 5hmC, and the relevant formulas are as follows: %5hmC = [tube 1× (tube 6/tube 3) − tube 4]/tube 6, %5mC = [tube 5 − tube 1× (tube 6/tube 3)]/tube 6. The statistics data from three independent experiments were used for generate the graphs.

Statistical analysis

All experiments were performed using three independent repeated experiments for cells. Unless otherwise indicated, data in the figures are presented as the mean ± SD. Statistical analyses were performed using Student's two-tailed unpaired *t* tests by GraphPad Prism 8.0 software (GraphPad Software) , unless otherwise specified. The *p* values < 0.05 are considered statistically significant and marked with asterisks ($^{*}p < 0.05$, $^{**}p < 0.01$, $^{***}p < 0.001$, $^{****}p < 0.0001$), as indicated in the figure legends.

Data availability

The mass spectrometry proteomics data have been deposited to the ProteomeXchange Consortium (http://proteomecentral.proteomexchange.org) *via* the iProX partner repository (63) with the dataset identifier PXD029415. The identified proteins were listed in Table S1.

Supporting information—This article contains supporting information.

Author contributions—R. W. conceptualization; Y. S. methodology; Y. S. software; J. Y. formal analysis; Y. S., T. J., L. R., W. H., Y. W., Z. P., and L. C. investigation; R. W. writing–review & editing; R. W. supervision.

Funding and additional information—Research was supported by grants from National Natural Science Foundation of China no. 81572903 (to R. W.) and Natural Science Foundation of Chongqing no. cstc2020jcyj-msxmX1094 (to J. Y.).

Conflict of interest—The authors declare that they have no conflicts of interest with the contents of this article.

Abbreviations—The abbreviations used are: 5-ghmC, glucosylated 5hmC; 5hmC, 5-hydroxymethylcytosine; 5mC, 5-methylcytosine; ChIP, chromatin immunoprecipitation; Co-IP, coimmunoprecipitation; CRC, colorectal cancer; DFO, deferoxamin; DFS, disease-free survival; DMC, differentially methylated CpG; DMOG, dimethyloxalylglycine; ES, enrichment score; FDR, false discovery rate; GluMS, glucosylated hydroxymethyl–sensitive; NES, normalized enrichment score; OS, overall survival; PLA, proximity ligation assay; qPCR, quatitative PCR; T4-BGT, T4 β-glucosyltransferase; TF, transcription factor; TSS, transcription start site.

References

1. Shimokawa, M., Ohta, Y., Nishikori, S., Matano, M., Takano, A., Fujii, M., *et al.* (2017) Visualization and targeting of LGR5^{+} human colon cancer stem cells. *Nature* **545**, 187–192
2. Jahanafrooz, Z., Mosafer, J., Akbari, M., Hashemzaei, M., Mokhtarzadeh, A., and Baradaran, B. (2020) Colon cancer therapy by focusing on colon cancer stem cells and their tumor microenvironment. *J. Cell Physiol.* **235**, 4153–4166
3. Zeuner, A., Todaro, M., Stassi, G., and De Maria, R. (2014) Colorectal cancer stem cells: from the crypt to the clinic. *Cell Stem Cell* **15**, 692–705
4. Zhang, Y., Kang, M., Zhang, B., Meng, F., Song, J., Kaneko, H., *et al.* (2019) m6A modification-mediated CBX8 induction regulates stemness and chemosensitivity of colon cancer *via* upregulation of LGR5. *Mol. Cancer* **18**, 185
5. van der Flier, L. G., van Gijn, M. E., Hatzis, P., Kujala, P., Haegebarth, A., Stange, D. E., *et al.* (2009) Transcription factor achaete scute-like 2 controls intestinal stem cell fate. *Cell* **136**, 903–912
6. Zhu, R., Yang, Y., Tian, Y., Bai, J., Zhang, X., Li, X., *et al.* (2012) Ascl2 knockdown results in tumor growth arrest by miRNA-302b-related inhibition of colon cancer progenitor cells. *PLoS one* **7**, e32170
7. Tian, Y., Pan, Q., Shang, Y., Zhu, R., Ye, J., Liu, Y., *et al.* (2014) MicroRNA-200 (miR-200) cluster regulation by achaete scute-like 2 (Ascl2): impact on the epithelial-mesenchymal transition in colon cancer cells. *J. Biol. Chem.* **289**, 36101–36115
8. Liu, X., Chen, X., Zhong, B., Wang, A., Wang, X., Chu, F., *et al.* (2014) Transcription factor achaete-scute homologue 2 initiates follicular T-helper-cell development. *Nature* **507**, 513–518
9. Takao, T., Asanoma, K., Tsunematsu, R., Kato, K., and Wake, N. (2012) The maternally expressed gene Tssc3 regulates the expression of MASH2 transcription factor in mouse trophoblast stem cells through the AKT-Sp1 signaling pathway. *J. Biol. Chem.* **287**, 42685–42694
10. Shang, Y., Pan, Q., Chen, L., Ye, J., Zhong, X., Li, X., *et al.* (2015) Achaete scute-like 2 suppresses CDX2 expression and inhibits intestinal neoplastic epithelial cell differentiation. *Oncotarget* **6**, 30993–31006
11. Ye, J., Liu, S., Shang, Y., Chen, H., and Wang, R. (2018) R-spondin1/Wnt-enhanced Ascl2 autoregulation controls the self-renewal of colorectal cancer progenitor cells. *Cell Cycle* **17**, 1014–1025
12. Wei, X., Ye, J., Shang, Y., Chen, H., Liu, S., Liu, L., *et al.* (2017) Ascl2 activation by YAP1/KLF5 ensures the self-renewability of colon cancer progenitor cells. *Oncotarget* **8**, 109301–109318
13. Shang, Y., Chen, H., Ye, J., Wei, X., Liu, S., and Wang, R. (2017) HIF-1α/Ascl2/miR-200b regulatory feedback circuit modulated the

epithelial-mesenchymal transition (EMT) in colorectal cancer cells. *Exp. Cell Res.* **360**, 243–256
14. Baylin, S. B., and Jones, P. A. (2016) Epigenetic determinants of cancer. *Cold Spring Harb. Perspect. Biol.* **8**, a019505
15. Shen, H., and Laird, P. W. (2013) Interplay between the cancer genome and epigenome. *Cell* **153**, 38–55
16. Smith, J., Sen, S., Weeks, R. J., Eccles, M. R., and Chatterjee, A. (2020) Promoter DNA hypermethylation and paradoxical gene activation. *Trends Cancer* **6**, 392–406
17. Lee, D. D., Leão, R., Komosa, M., Gallo, M., Zhang, C. H., Lipman, T., *et al.* (2019) DNA hypermethylation within TERT promoter upregulates TERT expression in cancer. *J. Clin. Invest.* **129**, 223–229
18. Curradi, M., Izzo, A., Badaracco, G., and Landsberger, N. (2002) Molecular mechanisms of gene silencing mediated by DNA methylation. *Mol. Cell Biol.* **22**, 3157–3173
19. Wu, H., and Zhang, Y. (2014) Reversing DNA methylation: mechanisms, genomics, and biological functions. *Cell* **156**, 45–68
20. Das, P. M., and Singal, R. (2004) DNA methylation and cancer. *J. Clin. Oncol.* **22**, 4632–4642
21. Tajbakhsh, J., Stefanovski, D., Tang, G., Wawrowsky, K., Liu, N., and Fair, J. H. (2015) Dynamic heterogeneity of DNA methylation and hydroxymethylation in embryonic stem cell populations captured by single-cell 3D high-content analysis. *Exp. Cell Res.* **332**, 190–201
22. Juelich, T., Sutcliffe, E. L., Denton, A., He, Y., Doherty, P. C., Parish, C. R., *et al.* (2009) Interplay between chromatin remodeling and epigenetic changes during lineage-specific commitment to granzyme B expression. *J. Immunol.* **183**, 7063–7072
23. Rasmussen, K. D., Jia, G., Johansen, J. V., Pedersen, M. T., Rapin, N., Bagger, F. O., *et al.* (2015) Loss of TET2 in hematopoietic cells leads to DNA hypermethylation of active enhancers and induction of leukemogenesis. *Genes Dev.* **29**, 910–922
24. Kohli, R. M., and Zhang, Y. (2013) TET enzymes, TDG and the dynamics of DNA demethylation. *Nature* **502**, 472–479
25. Delhommeau, F., Dupont, S., Della Valle, V., James, C., Trannoy, S., Massé, A., *et al.* (2009) Mutation in TET2 in myeloid cancers. *N. Engl. J. Med.* **360**, 2289–2301
26. Langemeijer, S. M., Aslanyan, M. G., and Jansen, J. H. (2009) TET proteins in malignant hematopoiesis. *Cell Cycle* **8**, 4044–4048
27. Ko, M., Huang, Y., Jankowska, A. M., Pape, U. J., Tahiliani, M., Bandukwala, H. S., *et al.* (2010) Impaired hydroxylation of 5-methylcytosine in myeloid cancers with mutant TET2. *Nature* **468**, 839–843
28. Kudo, Y., Tateishi, K., Yamamoto, K., Yamamoto, S., Asaoka, Y., Ijichi, H., *et al.* (2012) Loss of 5-hydroxymethylcytosine is accompanied with malignant cellular transformation. *Cancer Sci.* **103**, 670–676
29. Xu, Y. P., Lv, L., Liu, Y., Smith, M. D., Li, W. C., Tan, X. M., *et al.* (2019) Tumor suppressor TET2 promotes cancer immunity and immunotherapy efficacy. *J. Clin. Invest.* **129**, 4316–4331
30. Vasanthakumar, A., and Godley, L. A. (2015) 5-hydroxymethylcytosine in cancer: significance in diagnosis and therapy. *Cancer Genet.* **208**, 167–177
31. Figueroa, M. E., Abdel-Wahab, O., Lu, C., Ward, P. S., Patel, J., Shih, A., *et al.* (2010) Leukemic IDH1 and IDH2 mutations result in a hypermethylation phenotype, disrupt TET2 function, and impair hematopoietic differentiation. *Cancer Cell* **18**, 553–567
32. Hon, G. C., Song, C. X., Du, T., Jin, F., Selvaraj, S., Lee, A. Y., *et al.* (2014) 5mC oxidation by Tet2 modulates enhancer activity and timing of transcriptome reprogramming during differentiation. *Mol. Cell* **56**, 286–297
33. Lu, F., Liu, Y., Jiang, L., Yamaguchi, S., and Zhang, Y. (2014) Role of Tet proteins in enhancer activity and telomere elongation. *Genes Dev.* **28**, 2103–2119
34. Sardina, J. L., Collombet, S., Tian, T. V., Gómez, A., Di Stefano, B., Berenguer, C., *et al.* (2018) Transcription factors drive Tet2-mediated enhancer demethylation to reprogram cell fate. *Cell Stem Cell* **23**, 727–741.e9
35. Verma, N., Pan, H., Doré, L. C., Shukla, A., Li, Q. V., Pelham-Webb, B., *et al.* (2018) TET proteins safeguard bivalent promoters from de novo methylation in human embryonic stem cells. *Nat. Genet.* **50**, 83–95
36. Thomson, J. P., Ottaviano, R., Unterberger, E. B., Lempiäinen, H., Muller, A., Terranova, R., *et al.* (2016) Loss of Tet1-associated 5-hydroxymethylcytosine is concomitant with aberrant promoter hypermethylation in liver cancer. *Cancer Res.* **76**, 3097–3108
37. Margalit, S., Avraham, S., Shahal, T., Michaeli, Y., Gilat, N., Magod, P., *et al.* (2020) 5-Hydroxymethylcytosine as a clinical biomarker: Fluorescence-based assay for high-throughput epigenetic quantification in human tissues. *Int. J. Cancer* **146**, 115–122
38. Jubb, A. M., Chalasani, S., Frantz, G. D., Smits, R., Grabsch, H. I., Kavi, V., *et al.* (2006) Achaete-scute like 2 (ascl2) is a target of Wnt signalling and is upregulated in intestinal neoplasia. *Oncogene* **25**, 3445–3457
39. Strubberg, A. M., Veronese Paniagua, D. A., Zhao, T., Dublin, L., Pritchard, T., Bayguinov, P. O., *et al.* (2018) The zinc finger transcription factor PLAGL2 enhances stem cell fate and activates expression of ASCL2 in intestinal epithelial cells. *Stem Cell Rep.* **11**, 410–424
40. Novellasdemunt, L., Antas, P., and Li, V. S. (2015) Targeting Wnt signaling in colorectal cancer. A review in the theme: cell signaling: proteins, pathways and mechanisms. *Am. J. Physiol. Cell Physiol.* **309**, C511–521
41. Kasof, G. M., Goyal, L., and White, E. (1999) Btf, a novel death-promoting transcriptional repressor that interacts with Bcl-2-related proteins. *Mol. Cell Biol.* **19**, 4390–4404
42. Giakountis, A., Moulos, P., Zarkou, V., Oikonomou, C., Harokopos, V., Hatzigeorgiou, A. G., *et al.* (2016) A positive regulatory loop between a Wnt-regulated non-coding RNA and ASCL2 controls intestinal stem cell fate. *Cell Rep.* **15**, 2588–2596
43. Levin, B., Lieberman, D. A., McFarland, B., Andrews, K. S., Brooks, D., Bond, J., *et al.* (2008) Screening and surveillance for the early detection of colorectal cancer and adenomatous polyps, 2008: a joint guideline from the American cancer society, the US multi-society task force on colorectal cancer, and the American college of radiology. *Gastroenterology* **134**, 1570–1595
44. Gupta, R., Bhatt, L. K., Johnston, T. P., and Prabhavalkar, K. S. (2019) Colon cancer stem cells: potential target for the treatment of colorectal cancer. *Cancer Biol. Ther.* **20**, 1068–1082
45. Batlle, E., and Clevers, H. (2017) Cancer stem cells revisited. *Nat. Med.* **23**, 1124–1134
46. Du, X., Dong, Y., Shi, H., Li, J., Kong, S., Shi, D., *et al.* (2014) Mst1 and mst2 are essential regulators of trophoblast differentiation and placenta morphogenesis. *PLoS One* **9**, e90701
47. Cowden Dahl, K. D., Fryer, B. H., Mack, F. A., Compernolle, V., Maltepe, E., Adelman, D. M., *et al.* (2005) Hypoxia-inducible factors 1alpha and 2alpha regulate trophoblast differentiation. *Mol. Cell Biol.* **25**, 10479–10491
48. Renaud, S. J., Chakraborty, D., Mason, C. W., Rumi, M. A., Vivian, J. L., and Soares, M. J. (2015) OVO-like 1 regulates progenitor cell fate in human trophoblast development. *Proc. Natl. Acad. Sci. U. S. A.* **112**, E6175–6184
49. Basu, S., Gavert, N., Brabletz, T., and Ben-Ze'ev, A. (2018) The intestinal stem cell regulating gene ASCL2 is required for L1-mediated colon cancer progression. *Cancer Lett.* **424**, 9–18
50. Schuijers, J., Junker, J. P., Mokry, M., Hatzis, P., Koo, B. K., Sasselli, V., *et al.* (2015) Ascl2 acts as an R-spondin/Wnt-responsive switch to control stemness in intestinal crypts. *Cell Stem Cell* **16**, 158–170
51. Kwon, O. H., Park, J. L., Baek, S. J., Noh, S. M., Song, K. S., Kim, S. Y., *et al.* (2013) Aberrant upregulation of ASCL2 by promoter demethylation promotes the growth and resistance to 5-fluorouracil of gastric cancer cells. *Cancer Sci.* **104**, 391–397
52. Heclo, H. (1995) The clinton health plan: historical perspective. *Health Aff. (Millwood)* **14**, 86–98
53. Bert, S. A., Robinson, M. D., Strbenac, D., Statham, A. L., Song, J. Z., Hulf, T., *et al.* (2013) Regional activation of the cancer genome by long-range epigenetic remodeling. *Cancer Cell* **23**, 9–22
54. Wu, X., and Zhang, Y. (2017) TET-mediated active DNA demethylation: mechanism, function and beyond. *Nat. Rev. Genet.* **18**, 517–534
55. Wu, M. Z., Chen, S. F., Nieh, S., Benner, C., Ger, L. P., Jan, C. I., *et al.* (2015) Hypoxia drives breast tumor malignancy through a TET-TNFα-p38-MAPK signaling axis. *Cancer Res.* **75**, 3912–3924

56. Liu, J., Jiang, J., Mo, J., Liu, D., Cao, D., Wang, H., *et al.* (2019) Global DNA 5-hydroxymethylcytosine and 5-formylcytosine contents are decreased in the early stage of hepatocellular carcinoma. *Hepatology* **69**, 196–208
57. Huang, Y., Wang, G., Liang, Z., Yang, Y., Cui, L., and Liu, C. Y. (2016) Loss of nuclear localization of TET2 in colorectal cancer. *Clin. Epigenet.* **8**, 9
58. Ko, M., An, J., Bandukwala, H. S., Chavez, L., Aijö, T., Pastor, W. A., *et al.* (2013) Modulation of TET2 expression and 5-methylcytosine oxidation by the CXXC domain protein IDAX. *Nature* **497**, 122–126
59. Chen, Q., Chen, Y., Bian, C., Fujiki, R., and Yu, X. (2013) TET2 promotes histone O-GlcNAcylation during gene transcription. *Nature* **493**, 561–564
60. Zhou, X., Li, X., Cheng, Y., Wu, W., Xie, Z., Xi, Q., *et al.* (2014) BCLAF1 and its splicing regulator SRSF10 regulate the tumorigenic potential of colon cancer cells. *Nat. Commun.* **5**, 4581
61. Lee, S. H., Kalejta, R. F., Kerry, J., Semmes, O. J., O'Connor, C. M., Khan, Z., *et al.* (2012) BclAF1 restriction factor is neutralized by proteasomal degradation and microRNA repression during human cytomegalovirus infection. *Proc. Natl. Acad. Sci. U. S. A.* **109**, 9575–9580
62. Wen, Y., Zhou, X., Lu, M., He, M., Tian, Y., Liu, L., *et al.* (2019) Bclaf1 promotes angiogenesis by regulating HIF-1α transcription in hepatocellular carcinoma. *Oncogene* **38**, 1845–1859
63. Ma, J., Chen, T., Wu, S., Yang, C., Bai, M., Shu, K., *et al.* (2019) iProX: an integrated proteome resource. *Nucl. Acids Res.* **47**, D1211–D1217